THESIS

ASSESSING THE INFLUENCE OF MODEL INPUTS ON PERFORMANCE OF THE EMT+VS SOIL MOISTURE DOWNSCALING MODEL FOR A LARGE FOOTHILLS REGION IN NORTHERN COLORADO

Submitted by

Samantha C. Fischer

Department of Civil and Environmental Engineering

In partial fulfillment of the requirements

For the Degree of Master of Science

Colorado State University

Fort Collins, Colorado

Spring 2024

Master's Committee:

Advisor: Jeffrey D. Niemann
Co-Advisor: Joseph Scalia

Lisa Stright

ABSTRACT

ASSESSING THE INFLUENCE OF MODEL INPUTS ON PERFORMANCE OF THE EMT+VS SOIL MOISTURE DOWNSCALING MODEL FOR A LARGE FOOTHILLS REGION IN NORTHERN COLORADO

Soil moisture is an important driving variable of the hydrologic cycle and a key consideration for decision-making in off-road vehicle mobility, crop modeling, drought forecasting, flood prediction, and a variety of other applications. Soil moisture can be estimated at coarse resolutions (>1 km) using satellite remote sensing or land surface models; however, coarse resolution estimates are unsuitable for many applications. Downscaling these products to finer resolutions (~10 m) creates soil moisture maps that are more useful. This study applies the Equilibrium Moisture from Topography, Vegetation, and Soil (EMT+VS) model to Maxwell Ranch, a 4,000-ha cattle ranch in Northern Colorado that represents a diverse range of topographic, vegetation, and soil characteristics and a wide range of soil moisture conditions. The EMT+VS model is a physically based geo-information method that downscales coarse resolution soil moisture estimates using ancillary fine resolution datasets of topography and vegetation. Input data to the EMT+VS model contain inherent sources of error that can impact the uncertainty of downscaled estimates.

The objective of this study is to identify sources of uncertainty in inputs and assess their influence on the error of the EMT+VS model output. The study finds changes in vegetation input or digital elevation model (DEM) resolution introduce substantial errors in the EMT+VS model

output; however, these errors can be mostly overcome when recalibration with local in-situ data is possible. The highest errors (RMSE = 0.20 cm^3/cm^3) tend to occur in locations with thick vegetation and high contributing area, which are difficult to accurately estimate with available remote sensing data sources.

ACKNOWLEDGEMENTS

With gratitude I acknowledge the Leonard Wood Institute and the Army Research Laboratory for sponsoring this project. I also thank my advisors Dr. Jeffrey Niemann and Dr. Joseph Scalia, as well as Tim Green, for their guidance throughout this project. I am also grateful to Dr. Lisa Stright for serving on my master's committee. I acknowledge Joel Vaad for coordinating access to Maxwell Ranch and Matthew Bullock, Holly Proulx, Boran Kim, Muhammad Ukasha, Joe Bindner, Samuel Jacob, and Heath Orcutt for their assistance with field data collection. I also thank John Eylander and Adam Sisco for providing GeoWATCH data.

TABLE OF CONTENTS

1 INTRODUCTION

Soil moisture (volumetric water content) is an important variable in the hydrologic cycle, driving various atmospheric, hydrologic, and biological processes (Legates et al., 2011). Fine resolution maps of soil moisture provide useful information for various applications such as drought forecasting (Hirschi et al., 2011), flood prediction (Komma et al., 2008), agricultural production (Krishnan et al., 2006; Ines et al., 2013), and off-road vehicle mobility (Pundir & Garg, 2022). Fine resolution (3-30 m) soil moisture data required for these applications can be achieved through downscaling existing coarse resolution (~1-50 km) data. Satellite remote sensing, land-surface models (LSMs), or an average of measurements from an in-situ data network can be used as coarse resolution soil moisture from which to downscale.

Satellite Microwave Remote Sensing Platforms

There are several satellite microwave remote sensing platforms in use dedicated to monitoring surface soil moisture. The Soil Moisture Active Passion (SMAP) mission, launched by NASA in 2015, continuously monitors global soil moisture through passive microwave remote sensing using an L-band radiometer. SMAP's baseline mission requirement is to provide estimates of soil moisture in the top 5 cm of soil with an error no greater than 0.04 cm^3/cm^3 at a 10 km spatial resolution with 3-day average intervals globally, with some landcover exclusions (Entekhabi et al., 2014). This accuracy has been upheld according to numerous studies that have validated select passive, active-passive, and passive-enhanced products (Zeng et al., 2016; Chen et al., 2017; Chan et al., 2018). Chen et al. (2017) compared the performance of four SMAP radar and/or radiometer products at the Little Washita Watershed in Oklahoma and found that the Level 3 passive enhanced product had the lowest error, with an unbiased root mean square error

(RMSE) of 0.026 cm^3/cm^3. However, other SMAP products have been developed, such as the Level 2 SMAP radiometer/Copernicus Sentinel-1 soil moisture product and the Level 4 model-based product, which differ in method of retrieval, use of ancillary datasets, spatial resolution, accuracy, and temporal coverage (Das et al., 2019, 2020; Reichle et al., 2021) and therefore have different sources of error.

The Soil Moisture Ocean Salinity (SMOS) missions was launched by the European Space Agency (ESA) in early November 2009 and continues to provide global soil moisture estimates. Like SMAP, SMOS uses an L-band radiometer and aims to retrieve soil moisture data with a spatial resolution of 50 km or less and a revisit time of less than 3 days (Kerr et al., 2010). The Advanced Scatterometer, or ASCAT, is a real aperture radar instrument that uses backscatter data to derive soil moisture retrievals and is used onboard various satellite missions, primarily the MetOp satellite series (Bartalis et al., 2007). The spatial resolution of ASCAT ranges from approximately 25 to 50 km, achieving daily near-global coverage since initial launch of MetOp-A in 2007, with increasing coverage since the addition of more satellites (Wagner et al., 2013; Brocca et al., 2017). The Advanced Microwave Scanning Radiometer 2 (AMSR2), launched in May 2012 onboard the Global Change Observation Mission-Water (GCOM-W) satellite, is the successor to other AMSR instruments. GCOM-W uses a microwave radiometer to retrieve global soil moisture coverage every 2-3 days at a spatial resolution of 0.25° (~25 km) (Imaoka et al, 2010, Burgin et al. 2017).

Burgin et al. (2017) compared SMAP passive soil moisture products with other existing satellite products including SMOS, ASCAT, and AMSR2. They found that SMOS provided measurements most similar to SMAP, whereas ASCAT tended to predict wetter than SMAP and AMSR2 tended to predict drier, except in desert regions. All these satellite products are useful

for observing soil moisture consistently across a global scale at coarse resolutions, but they use different sensors, resolutions, and data collection techniques that yield deviations between soil moisture estimates.

Land Surface Models

Land surface models (LSMs) are also commonly used to simulate physical or biophysical processes on the earth's surface, including modeling the water balance. A wealth of LSMs exist that can be applied at regional or global scales to model soil moisture at various depths. The complexity and considerations involved in LSMs vary, but oftentimes these models consider a combination of meteorological data, soil properties, vegetation cover, land use, and topography. Koster et al. (2009) compared seven land surface models from the second phase of the Global Soil Wetness Project (GSWP-2) and found that the differences in modeled global soil moisture were substantial, despite using the same driving meteorological variables. However, different models generally captured the same temporal variability of soil moisture. Therefore, despite differences in the estimates across models, the relationship of one model to another could be characterized by a transformation, rather than interpreting the modeled soil moisture as a direct estimate. Implicit uncertainties in LSMs are also due to the coarse resolution (~100 km) of these models. On a more regional scale, the second phase of the North American Land Data Assimilation System (NLDAS-2) database includes soil moisture data from four land surface models: Noah, Mosaic, Sacramento soil moisture accounting (SAC), and Variable Infiltration Capacity (VIC) at a $1/8^{th}$ degree grid spacing (~12 km). Xia et al. (2015) evaluated these four LSMs against soil moisture observations from hundreds of sites across several U.S. states and found, while all models could generally capture seasonal variation in soil moisture, affirming the study by Koster et al., 2009, Mosaic demonstrated the lowest error for estimates in Colorado.

Furthermore, Xia et al., (2015) found that both SAC and Mosaic tended to estimate drier than the observations, whereas Noah and VIC tended to estimate wetter.

In-situ Soil Moisture

In-situ soil moisture data are collected using sensors or probes inserted or permanently installed in the ground to measure soil moisture in a natural environment in real time. In-situ sensors provide accurate measurements of soil moisture at a specific location, but these types of measurements are not available on a global scale. However, there are various experimental watersheds or expansive in-situ networks that exist in different regions throughout the world, which are useful for providing an abundance of data for use in hydrologic models or to validate soil moisture estimates from satellites (Gruber et al., 2013; Colliander et al., 2017), LSMs models (Caldwell et al., 2019), or downscaling models (Grieco et al., 2018; Gambill et al., 2020). These in-situ networks are usually intended to measure average, or "typical", conditions, and the average estimate from the network is used to validate the accuracy coarse-resolution estimates. As such, however, in situ networks typically do not capture the full range of conditions at a site and therefore leave out potentially critical information for many applications, particularly for mobility assessments.

Previous Efforts in Soil Moisture Downscaling

Downscaling methods take advantage of widely used, readily available, and temporally frequent coarse resolution soil moisture data from sources such as remote sensing platforms, LSMs, or in-situ network averages. Various downscaling (a.k.a. disaggregation) methods exist, which vary in their data inputs, methodologies, and output resolutions. Recent overviews of existing downscaling methods can be found in Peng et al. (2017), Ajami & Sharma (2018), and Sabaghy et al. (2020).

Radar-based downscaling is commonly used on a global scale, which fuses active (radar) and passive (radiometer) microwave data. These algorithms combine the benefit of frequent passive observations with higher resolution, but less frequent, active radar measurements. For example, the SMAP/Sentinel-1 L2 Radiometer/Radar product derives brightness temperatures from SMAP's 36 km radiometer and uses Sentinel-1 radar backscatter data to disaggregate them to higher resolution (3 km and 1 km) soil moisture retrievals (Das et al., 2019, 2020). Radar-based methods are useful for downscaling continuously and over large extents with exiting satellite data but provide outputs that are still too coarse (>1 km) for certain applications.

Optical/thermal downscaling is another satellite-based downscaling method that combines the advantages of multiple data products, in this case optical and thermal data, which are typically available at finer resolutions (tens of meters). Optical data provides a vegetation index (VI), and thermal data provides land-surface temperatures (LST). The LST/VI space typically resembles a triangle or trapezoid shape, which is used to determine 'dry' and 'wet' edges and parameterize the linear relationship between LST and soil moisture. This method is commonly referred to as the triangle or trapezoid method (Moran et al., 1994). The Disaggregation based on Physical and Theoretical scale Change (DisPATCh) model is an example of an optical/thermal method that has been used to disaggregate SMOS and AMSR-E products to a 1 km resolution (Merlin et al., 2012). Alternatively, the OPTRAM method proposed by Sadeghi et al., (2017) uses solely optical data and is a direct estimation of soil moisture, rather than a downscaling method. OPTRAM calculates shortwave transformed reflectance (STR) from a satellite's shortwave infrared (SWIR) band, which is analogous to LST in the triangle/trapezoid method and produces downscaled estimates that match the resolution of

the optical data source. However, these methods are limited by the availability of clear sky imagery and are not applicable for continuous use on a global scale.

Statistical approaches are also commonly used, which aim to preserve statistical properties of empirical soil moisture observations across scales (Mascaro et al. 2010, Deshon et al., 2020). Empirical Orthogonal Function (EOF) analysis is an example of a statistical method, which can be used to downscale soil moisture based on statistical relationships with observed properties, such as topography (Busch and Niemann, 2012). In recent work, machine learning has also been increasingly common for soil moisture downscaling. Commonly used machine learning algorithms include artificial neural network (ANN) (Xu et al., 2021; Alemohammad, 2018), Support Vector (Ahmad et al., 2010; Jin et al., 2020), regression trees (Wei, Z. et al., 2019, Liu et al., 2020b), and the Random Forest (RF) model (Zhao et al., 2018; Chen et al., 2020). Liu et al. (2020a), Srivastava et al. (2013), and Im et al. (2016) compared different machine learning techniques for viability in downscaling satellite soil moisture.

While statistical and machine learning methods rely on empirical relationships, geo-information methods use fine resolution ancillary data (such as topography, vegetation, or soil data) and their physical influence on soil moisture to inform the downscaling process (Busch et al., 2012; Werbylo and Niemann, 2014; Schröter et al., 2017). GeoWATCH is an example of a geo-information method that estimates high-resolution global soil moisture based on data assimilation from static (land use, soil texture, and DEM) and dynamic (meteorological variables) datasets (Eylander et al., 2023). GeoWATCH ingests coarse resolution (~10 km) data from the United States Air Force (USAF) 555th Weather Wing (557WW), which uses the Noah LSM, as a base estimate of soil moisture. The GeoWATCH downscaling algorithm is based on the STOPMODEL approach, which considers flow within shallow soils based on topographic

attributes (Walter et al., 2002). GeoWATCH produces 30-90 m resolution, soil moisture maps every 3-hours for the near-surface layer of 0–10 cm (Eylander et al., 2023). GeoWATCH downscaled estimates have been compared to catchment studies at Tarrawarra and Shale Hills where the modeled soil moisture outperformed the TDR average on most dates (Eylander et al., 2023). Additionally, GeoWATCH has been evaluated against USDA Soil Climate Analysis Network (SCAN) in-situ soil moisture measurements across 34 states. GeoWATCH had a lower RMSE for clayey soils (0.08 cm^3/cm^3) and a higher RMSE for sandy soils (0.11 cm^3/cm^3) (Gambill et al. 2020). While GeoWATCH has been evaluated at a small catchment-scale and a large regional scale, the algorithm performance has not yet been assessed at large study regions with high-resolution soil moisture networks, which might better showcase the effects of variations in terrain (Eylander et al., 2023).

This study focuses on the application of a geo-information method called the Equilibrium Moisture from Topography (EMT), Vegetation, and Soil (+VS) model. The original EMT model considered the dependence of soil moisture on topographic attributes. The model captured valley-dependent patterns, showing wetter conditions tend to occur in valley bottoms, as well as hillslope-dependent patterns, in which wetter conditions tend to occur on slopes oriented away from the sun (Coleman et al., 2013). The EMT model was later amended to include vegetation and soil considerations. Ranney and Niemann (2015) found that model performance improves when fine resolution spatial vegetation data are used. The EMT+VS model has been successfully applied at a variety of sites that represent a wide range of climate and vegetation, characteristics. Instrumentation also varied from site to site, with either permanent installations or portable TDR measurements, and depths ranging from 5 cm to 30 cm. Climates have ranged from sub-humid catchments in Australia and New Zealand to semi-arid regions in Colorado,

collectively representing grasslands, shrublands, and forests (Ranney et al., 2015; Grieco et al., 2018; Pauly et al., 2020). Testing beyond the catchment scale was conducted at two large and extensively monitored SMAP validation sites – the mountainous Reynolds Creek and the alpine Tibetan Plateau (Cowley et. al, 2017; Grieco et al., 2018). Reynold's Creek boasts the most forest cover and greatest topographic relief of any of the sites studied thus far. At this site, Cowley et al. (2017) assessed the impacts of incorporating elevation-dependent variables, such as precipitation and potential evapotranspiration (PET), into the EMT+VS model and found that adding downscaled PET data improved model performance. The robustness of the EMT+VS model in a variety of environments is demonstrated by the prediction of soil moisture with a root-mean-squared error of ~0.03–0.06 (Table A1).

Additionally, the EMT+VS model is adaptable in that the model can intake any user-specified dataset or locally known information, and/or the model can be calibrated using local observations. Greico et al. (2018) tested the method on a variety of catchment and large-scale study sites to assess the model performance if using global datasets for parameterization instead of local calibration. The study found that, while using global datasets still provides reasonable performance, site-specific calibration, though not always practical to implement, results in better performance and captures greater spatial variability. Nonetheless, global datasets, local calibration, or a combination of both, can be implemented in the EMT+VS model.

Unlike methods that aim to reproduce statistical patterns in soil moisture, or machine learning methods that are based on empirical training data, the EMT+VS model is a physically based approach that aims to estimate soil moisture as physically accurate as possible. Werbylo et al. (2014) found that the EMT+VS model outperformed an EOF method when fewer locations for in-situ data were available. Statistical methods like EOF likely require very large in-situ

datasets to fine-tune performance, whereas the EMT+VS model is constrained by physical considerations and can more accurately predict soil moisture without extensive in-situ networks. Additionally, unlike optical-thermal methods that rely on clear-image satellite data such as Sentinel-2 for their predictions, EMT+VS can be used for all dates, regardless of cloud cover.

Although the EMT+VS model has been tested extensively and successfully, further testing of model robustness to different landscape features is warranted as is exploration of the impact of varying input datasets on performance. This testing is needed to expand the applicability of the EMT+VS model to a wider variety of sites and data sources. Additionally, the EMT+VS model has not yet been tested in a realistic application scenario. Prior testing has been conducted in small catchments (Deshon et al., 2020), or with sparse in-situ networks across very large regions (Hoehn et al., 2017; Grieco et al., 2018). These studies have primarily used in-situ spatial average soil moisture and field measurements of vegetation, which are not practical to collect in any given region. Instead, using remote sensing data for these features may allow for more expansive use of the EMT+VS model. However, while the use of remote sensing data as inputs to the model will expand model usefulness, these data will have inherent errors that may propagate through the model and impact the error in the fine scale soil moisture estimates. So far, there has been limited consideration of the sources of error in these remote sensing platforms and the subsequent error caused when they are applied to the EMT+VS model.

The overarching purpose of this study is to (1) to evaluate the performance of the EMT+VS model when applied to a realistic field scale (approximately the size of a satellite coarse resolution grid cell) using an in-situ validation dataset that captures spatial variability of topography, vegetation, and soil and (2) to determine how the choice of inputs (including coarse resolution soil moisture, vegetation data, and topography data) affect the model performance.

2 METHODOLOGY

The EMT+VS model estimates fine resolution soil moisture for a specific date based on the coarse resolution average soil moisture and fine resolution data for topography and vegetation. The model can also use fine resolution data for soil properties, but Ranney et al. (2015) found only small improvements in the accuracy when fine resolution soil properties are considered.

The EMT+VS model estimates the fine resolution soil moisture using a water balance for the uppermost soil layer. The model considers four processes in the water balance: infiltration, deep drainage, lateral flow, and evapotranspiration (ET). Infiltration F (mm/day) is estimated based on a coarse resolution precipitation $\bar{P}$ (which eventually cancels out of the model) and an interception loss:

$$F = \bar{P}(1 - \lambda V) \tag{1}$$

where λ is an interception efficiency parameter and V is the fractional vegetation cover. Cowley et al. (2017) included a term describing orographic effects on precipitation and Pauly et al. (2020) included a term that accounts for runoff production. However, neither term is used here because they both produced only small improvements in the accuracy of the soil moisture estimates from the model.

Deep drainage G (mm/day) is calculated from Darcy's Law assuming gravity controls the vertical hydraulic gradient, and the Campbell (1974) equation describes the unsaturated hydraulic conductivity. Deep drainage is calculated as:

$$G = K_{s,v}\left(\frac{\theta}{\phi + \chi V}\right)^{\gamma_v} \tag{2}$$

where $K_{s,v}$ is the vertical saturated hydraulic conductivity (mm/day), γ_v is the vertical pore disconnected index, θ is the soil moisture, ϕ is the bare soil porosity, and χ adjusts the bare soil porosity to account for organic matter. The parameter χ has not been considered in prior applications of the EMT+VS model but was added here because the application region includes locations with very dense vegetation mats that are underlain by peat. Peat soils can have very high porosity (Rezanezhad et al., 2016; Park et al., 2021) which is poorly represented by a calibrated and spatially constant porosity value that is meant to characterize nonorganic soils. Pauly et al. (2020) also considered a residual water content in the EMT+VS model, but this feature is also not included here because the addition produced little improvement in performance.

Lateral flow L (m^2 mm/day) is also derived from Darcy's Law and the Campbell (1974) equation for unsaturated hydraulic conductivity. In this case, the hydraulic gradient is a function of the topographic slope, and the thickness of the soil layer is a function of topographic curvature. The resulting expression is:

$$L = \delta_0 \left(\frac{\kappa_{min} - \kappa}{\kappa_{min}}\right) c\iota K_{s,v} \left(\frac{\theta}{\phi + \chi V}\right)^{\gamma_h} S^{\epsilon} \quad (3)$$

where δ_0 is the layer thickness (m) where topographic curvature is zero, κ is the topographic curvature, κ_{min} is the minimum topographic curvature that has a soil layer, c (m) is the length of the digital elevation model (DEM) grid cells (and the final downscaled soil moisture grid cells), ι is the anisotropy of saturated hydraulic conductivity, γ_h is the horizontal pore disconnectedness index, S is the topographic slope, and ϵ is a parameter relating the hydraulic gradient to the topographic slope.

Evaporation and transpiration (ET) E (mm/day) is determined using the expression:

$$E = \overline{E_p}[1 + \omega(\bar{Z} - Z)][\eta V + (1 - V)^{\mu}]\left[\frac{I_p}{1+\alpha}\left(\frac{\theta}{\phi+\chi V}\right)^{\beta_r} + \frac{\alpha}{1+\alpha}\left(\frac{\theta}{\phi+\chi V}\right)^{\beta_a}\right] \quad (4)$$

where E_p is a coarse resolution potential ET (mm/day). The term $[1 + \omega(\bar{Z} - Z)]$ adds fine resolution variations to the potential ET based on elevation. The parameter ω controls the elevation dependence, Z is the local elevation (m), and $\bar{Z}$ is average elevation in the coarse resolution grid cell. The term $[\eta V + (1 - V)^{\mu}]$ describes the effect of fractional vegetation cover on the transpiration and evaporation. The parameter η is the portion of the transpiration that comes from the modeled soil layer and μ describes the effect of shading on soil evaporation. The final term in the ET equation describes the effects of topography and moisture limitations on ET. I_p is the potential solar radiation index (which depends on the topographic slope and aspect) (Lee, 1964; Swift, 1976; Dingman, 2015), α is the Priestly-Taylor coefficient minus one (Priestley & Taylor, 1972), and β_a and β_r describe the effects of moisture limitations on aerodynamic and radiative ET, respectively.

Coleman and Niemann (2013) developed a solution strategy that allows calculation of fine resolution soil moisture by assuming equilibrium. Four explicit analytical solutions for soil moisture were derived by assuming each outflow term dominates. The final soil moisture is a weighted average of the four analytical soil moisture estimates:

$$\theta = \frac{w_G\theta_G + w_L\theta_L + w_R\theta_R + w_A\theta_A}{w_G + w_L + w_R + w_A} \quad (5)$$

where θ_G, θ_L, θ_R, and θ_A are the analytical estimates if deep drainage, lateral flow, radiative ET, and aerodynamic ET, respectively, dominate the water balance. The weights w_G, w_L, w_R, and w_A are determined based on the actual magnitude of deep drainage, lateral flow, radiative ET, and aerodynamic ET in the water balance. The analytical soil moisture estimates are:

$$\theta_G = \bar{\theta}\frac{DDI}{\overline{DDI}} \quad (6)$$

$$\theta_L = \bar{\theta}\frac{LFI}{\overline{LFI}} \tag{7}$$

$$\theta_R = \bar{\theta}\frac{REI}{\overline{REI}} \tag{8}$$

$$\theta_A = \bar{\theta}\frac{AEI}{\overline{AEI}} \tag{9}$$

where $\bar{\theta}$ is the coarse resolution soil moisture, *DDI* is the deep drainage index, *LFI* is the lateral flow index, *REI* is the radiative ET index, and *AEI* is the aerodynamic ET index. The bar above each index in the denominators indicates the spatial average within the coarse grid cell. The *DDI*, *LFI*, *REI*, and *AEI* are fine resolution (temporally invariant) patterns that control the soil moisture pattern. They are calculated as:

$$DDI = (\phi + \chi V)\left(\frac{1-\lambda V}{K_{s,v}}\right)^{1/\gamma_v} \tag{10}$$

$$LFI = (\phi + \chi V)\left(\frac{1-\lambda V}{K_{s,v}}\right)^{1/\gamma_h}\left(\frac{A}{cS^{\epsilon}}\right)^{1/\gamma_h}\left(\frac{\kappa_{mn}}{\kappa_{min}-\kappa}\right)^{1/\gamma_h} \tag{11}$$

$$REI = (\phi + \chi V)\left\{\frac{1+\alpha}{\bar{E}_p[1+\omega(\bar{Z}-Z)]}\right\}^{1/\beta_r}\left(\frac{1}{I_p}\right)^{1/\beta_r}\left[\frac{1-\lambda V}{\eta V+(1-V)^{\mu}}\right]^{1/\beta_r} \tag{12}$$

$$AEI = (\phi + \chi V)\left\{\frac{1+\alpha}{\alpha\bar{E}_p[1+\omega(\bar{Z}-Z)]}\right\}^{1/\beta_a}\left[\frac{1-\lambda V}{\eta V+(1-V)^{\mu}}\right]^{1/\beta_a} \tag{13}$$

The weights associated with each analytical solution vary in time based on the coarse resolution soil moisture. These weights are calculated as:

$$w_G = \left(\frac{\bar{\theta}}{\overline{DDI}}\right)^{\gamma_v} \tag{14}$$

$$w_L = \left(\frac{\bar{\theta}}{\overline{LFI}}\right)^{\gamma_h} \tag{15}$$

$$w_R = \left(\frac{\bar{\theta}}{\overline{REI}}\right)^{\beta_r} \tag{16}$$

$$w_A = \left(\frac{\bar{\theta}}{\overline{AEI}}\right)^{\beta_a} \tag{17}$$

The mathematical structure of the EMT+VS model allows the spatial structure of the fine resolution soil moisture to vary as the coarse resolution soil moisture varies in time (Coleman and Niemann, 2013). However, the spatial structure does not consider any hysteresis in the soil moisture patterns (a given coarse resolution soil moisture always produces the same spatial structure in the fine resolution pattern).

3 APPLICATION TO STUDY REGION

3.1 Study Region

For this study, the EMT+VS model was applied at Maxwell Ranch, a 4,000-ha working cattle ranch located in Northern Colorado, approximately 53 km northwest of Fort Collins in the Laramie foothills. The site has an average elevation of 2,150 m and ~325 m of topographic relief, representing hilltops and plains. Soils in the region are predominantly coarse loamy soils (Soil Survey Staff, 2022). The climate at Maxwell Ranch is semiarid, with an annual potential ET of approximately 16 cm (Trabucca & Zomer, 2019) and an average annual rainfall of ~42 cm, according to historical data from a nearby weather station (location shown in Figure 1). Vegetation includes shrublands, short-grass prairies, and scattered ponderosa pine forests.

3.2 Datasets Used for Model Evaluation

An extensive soil moisture sampling campaign was conducted at Maxwell Ranch to collect data to evaluate the soil moisture estimates from the EMT+VS model. Four subregions — named Region A, B, C, and D (shown in Figure 1) — were specified to cluster sampling locations, which facilitated field data collection and allowed for a wide range of conditions to be observed throughout the ranch. Within each subregion, 18 to 22 sampling locations were selected (86 points total across the ranch), aiming to capture a diverse combination of topographic, vegetation, and soil conditions at the selected points. At each sampling location, three measurements were taken using a portable Stevens Water HydraProbe II, which uses coaxial impedance dielectric reflectometry to measure the average volumetric water content in the top 5 cm of the soil. According to the manufacturer, the HydraProbe provides soil moisture measurements with a high accuracy of ± 0.01 to 0.03, depending on soil type (Stevens Water,

2018). Additionally, an average of three measurements at each point was taken, which helps reduce randomness in the data.

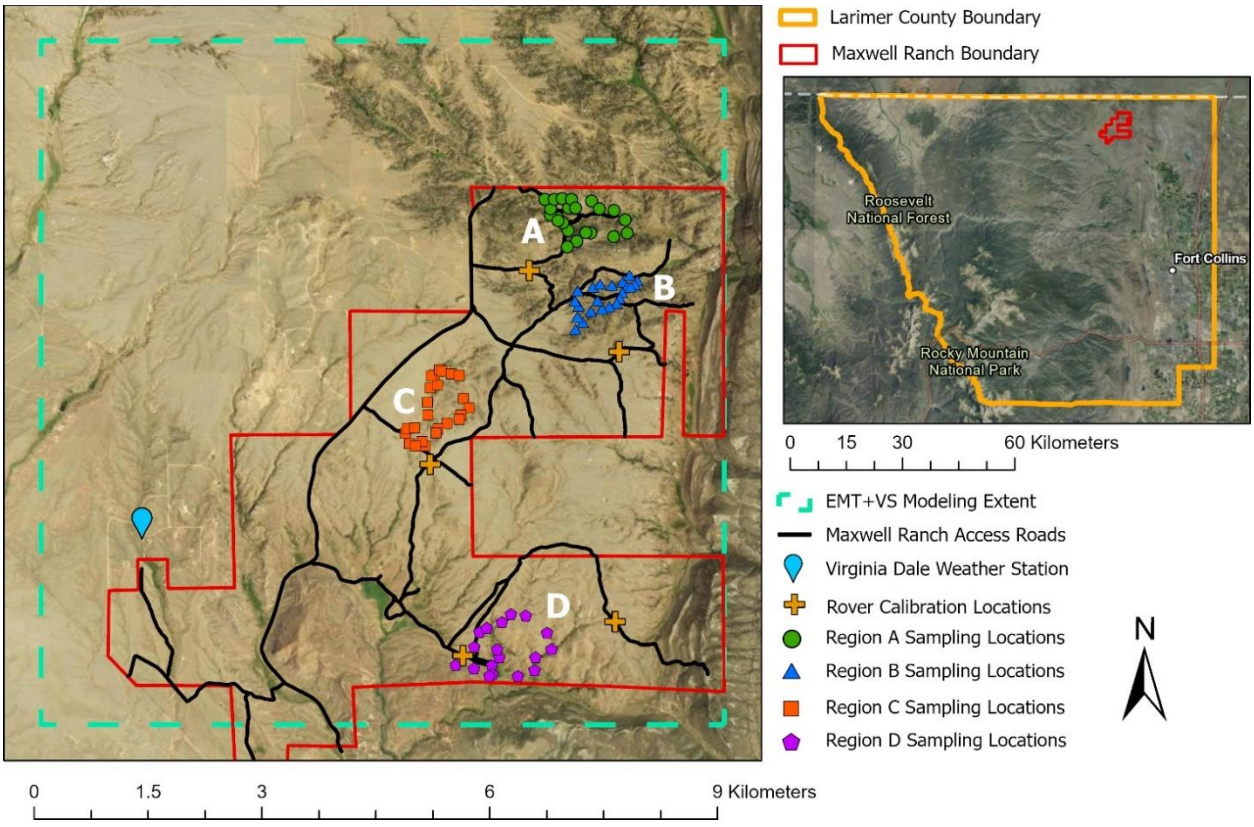

Figure 1. Map of Maxwell Ranch study region and four subregions where field data were collected. The modeling extent corresponds to the boundary of a 9 km SMAP Level 3 Enhanced Passive soil moisture grid cell.

Figure 2 shows daily total precipitation data throughout the study period, which was obtained from the nearby Virginia Dale weather station (shown on map in Figure 1). Field dates and their respective average soil moisture according to the HydraProbe site average are also indicated. Between the months of May and August 2023, data was collected at ten sampling dates that captured a variety of moisture conditions, including wetting and drying cycles in response to precipitation events. The sampling campaign was conducted during the summer to avoid the effects of snow, which are not considered by the model.

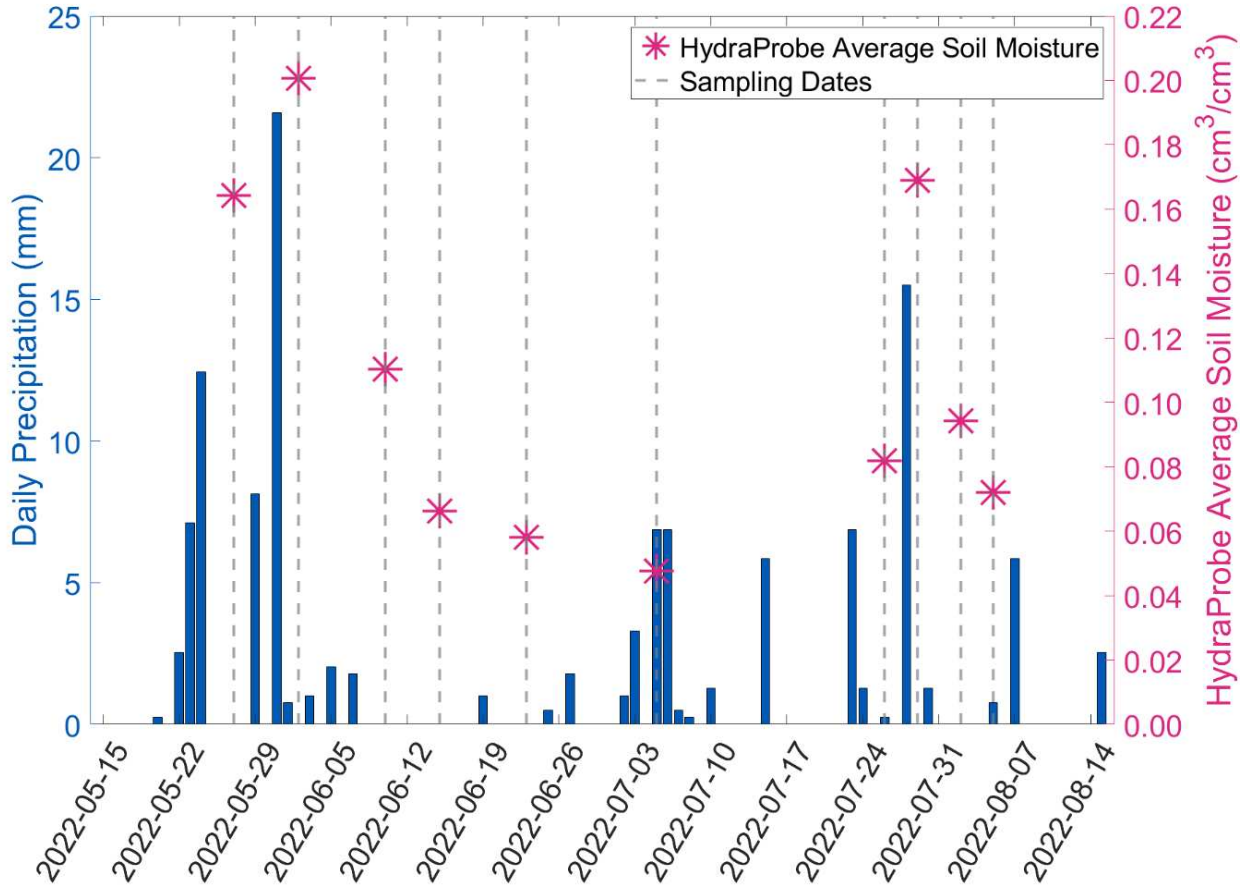

Figure 2. Precipitation recorded at Virginia Dale weather station (see location in Figure 1) during study period.

Average site soil moisture from the HydraProbe data generally follows the precipitation trends. The wettest sampling date occurred on 2 June after a substantial precipitation event on 31 May, which was followed by a drying cycle through 23 June. The next wettest sampling date, 29 July, was followed by another period of drying through 5 August.

4 MODEL INPUTS AND APPLICATION

Application of the EMT+VS model requires coarse resolution soil moisture and fine resolution topographic and vegetation data as inputs, which together provide spatial data for average soil moisture, elevation, slope, aspect, contributing area, curvature, potential solar radiation index (PSRI), and fractional vegetation cover. This section discusses inputs used in the EMT+VS model application at Maxwell Ranch.

4.1 Coarse resolution Soil Moisture

Daily Spatial Average of HydraProbe Measurements

In previous studies using the EMT+VS model (Coleman and Niemann, 2013; Werbylo and Niemann, 2014; Ranney et al., 2015; Cowley et al., 2017; Hoehn et al., 2017; Grieco et al., 2018; Pauly et al., 2020), the average of point data was used as the coarse resolution soil moisture input. The spatial averages of the HydraProbe measurements on each date were also used as a coarse resolution input in this study. However, because the points selected in this study are sparse and intended to capture a variety of conditions, the average of point data might not be representative of overall average conditions across the ranch, despite the point data itself having high accuracy.

Cosmic Ray Neutron Rover

In addition to HydraProbe data, a cosmic-ray neutron rover (CRNR), subsequently referred to as the 'rover,' was used to provide intermediate-scale soil moisture estimates during field data collection. A non-invasive technique to estimate soil moisture at an intermediate scale (hundreds of meters) using cosmic ray neutrons was first introduced by Zreda et al. (2008). Estimating soil moisture from cosmic rays is based off the relationship between neutron intensity

and hydrogen content. Cosmic-ray neutrons in soil are moderated, or slowed, by hydrogen atoms. Therefore, the intensity of neutron backscatter is inversely correlated to gravimetric water content. In other words, higher water content in the soil leads to more effective moderation of neutrons and thus lower backscatter intensities (Hendrick and Edge, 1966; Kodama et al., 1985). Cosmic-ray neutron sensing can be applied using stationary instruments that continuously monitor soil moisture over a large static footprint (Zreda et al., 2008; Fersch et al., 2020) or, as is the case with the rover used in this study, the sensor can be mounted on a ground-based vehicle to measure the spatial variability of soil moisture over large extents (Desilets et al., 2010; Schrön et al., 2018).

Calibration is required to determine the dry neutron count, N_0, which relates neutron counts from the cosmic ray neutron sensor to gravimetric water contents. At Maxwell Ranch, the rover was parked at five calibration locations (shown in Figure 1) while ~25 HydraProbe measurements were taken incrementally up to a radius of 60 m, which captures the area of the footprint with the strongest influence on total neutron counts (Köhli et al. 2015). Soil samples were collected at calibration locations to determine bulk densities used to convert between gravimetric water content and volumetric water content. N_0 was determined for each calibration location at each date so that the soil moisture from the rover matched the HydraProbe average within the footprint. A final site wide N_0 value of 1741 was determined by averaging N_0 values across all calibration locations and dates. This final N_0 was used in subsequent analysis to determine the soil moisture from the neutron counts collected by the rover throughout the ranch.

The rover was driven over ~43 km of access roads throughout Maxwell Ranch on each sampling date, capturing data along the path within a radius of ~290 m (footprint determined as a function of air pressure, vegetation height, and soil moisture according to Köhli et al., 2015).

Figure 3 shows the rover soil moisture estimates along the path, as well as the HydraProbe point measurements collected at Regions A, B, C, and D on the same field dates. Due to logistical challenges, HydraProbe data were not collected at two regions on two dates (27 May and 5 July), and the rover did not cover all roads on 27 May. In total, the final dataset includes a total of 775 HydraProbe observations (each the average of three measurements) and rover data along access roads across Maxwell Ranch.

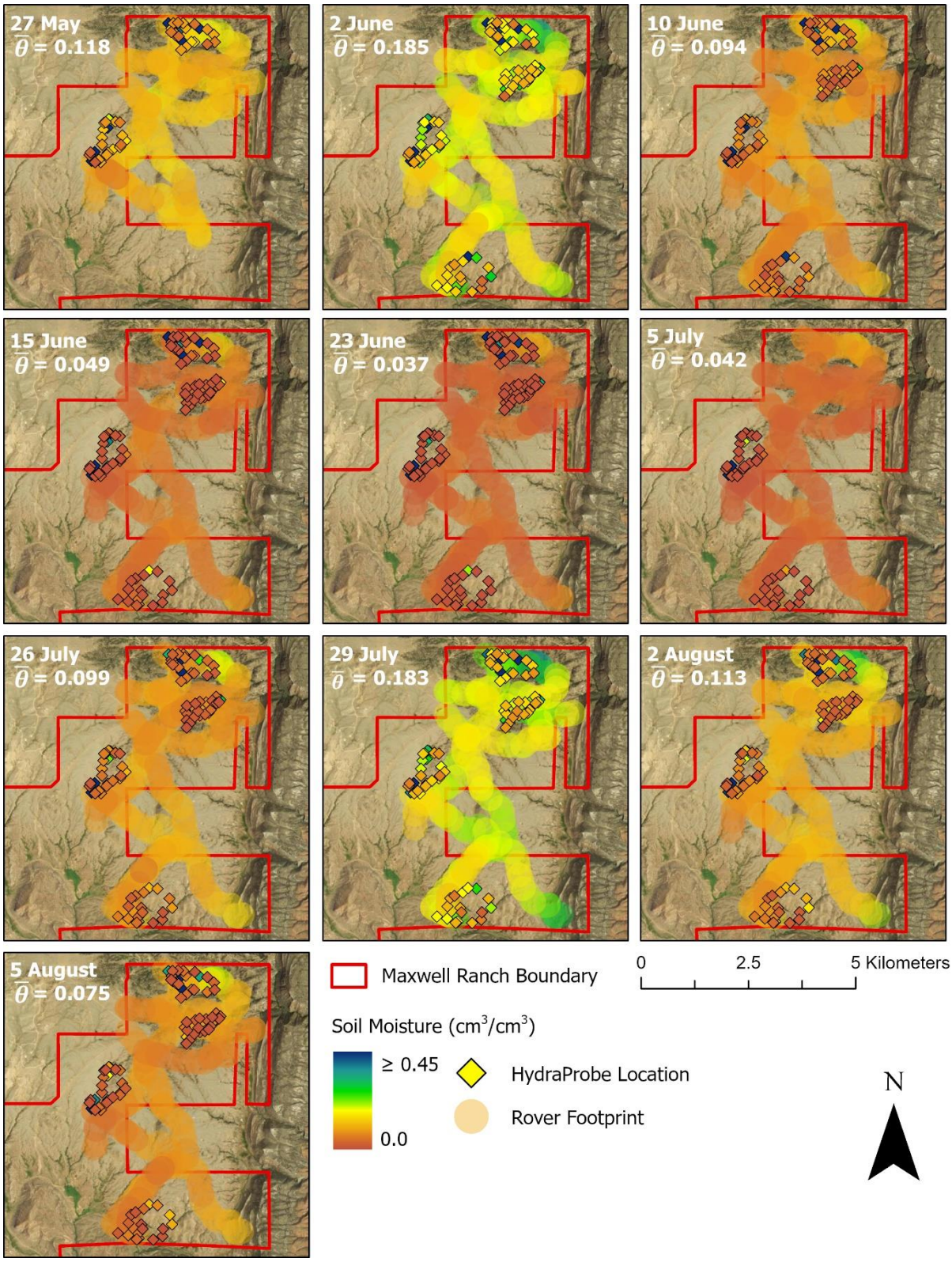

Figure 3. Maps of soil moisture measured with portable HydraProbes and a cosmic ray neutron rover on all sampling dates superimposed on satellite imagery of the study region. Average spatial soil moisture, $\bar{\theta}$, is calculated from the average of rover data.

As shown in Figure 3, the rover captures soil moisture conditions over a much larger extent than the HydraProbe measurements alone, occupying most of the eastern portion of the ranch. The rover average, because the instrument captures soil moisture across a larger extent, may be a better representation of average soil moisture conditions across the site than the average of the HydraProbe data. Therefore, the site-wide average of rover data on each date was also tested as a coarse resolution soil moisture input to the EMT+VS model.

Soil Moisture Active Passive (SMAP)

SMAP products are desirable due to their accessibility, spatial coverage, temporal coverage, and reported accuracy. These products have varying spatial and temporal resolutions depending on the specific product and the instruments used. For this study, only products with a 9 km resolution or smaller were selected because Maxwell Ranch is fully captured in a single grid cell (see 'Modeling Extent' in Figure 1); therefore, a single SMAP value may provide a reasonable estimate for the spatial average soil moisture estimate of the site. The products used were the Enhanced Level 3 Radiometer (L3_SM_P_E), the SMAP L4 surface soil moisture (L4_SM), and the Level 2 SMAP radiometer/Copernicus Sentinel-1 soil moisture (L2_SM_SP), all which output surface soil moisture in the top ~5 cm of the soil layer.

L3_SM_P_E provides daily estimates of global soil moisture on a 9 km grid through the combined use of the SMAP radiometer (36 km retrieval) and brightness temperature data at a 9 km resolution (Chan et al., 2018; O'Neill et al., 2021). For this study, L3_SM_P_E was obtained for each date and projected to NAD 1983 UTM 13. The value for the grid cell overlaying Maxwell Ranch, which corresponds with the modeling extent boundary shown in Figure 1, was used as the coarse resolution soil moisture input.

L4_SM, also available at a 9 km resolution, is a model-based product, which merges SMAP radiometer brightness temperature observations into a land surface model, producing global estimates at 3-hour time intervals (Reichle et al., 2021). Specifically, the 3-hr time block from UTC 15-18 was selected because the time range most closely corresponds with the approximate time frame in which field measurements were taken (~9:00am-12:00pm Mountain Standard Time). Again, the value of the grid cell overlaying Maxwell Ranch was used as the coarse soil moisture input.

L2_SM_SP merges SMAP radiometer data disaggregated by finer-resolution Sentinel-1 radar data, resulting in a finer-resolution product (3 km) (Das et al., 2019). However, L2_SM_SP lacks the temporal frequency of other products; although the SMAP radiometer has a 2–3-day revisit time, the Sentinel-1 orbit has a revisit frequency of ~12 days, which limits the overall temporal availability of this product and creates considerable gaps in the data. Between May and August 2022, the window for data collection at Maxwell Ranch, L2_SM_SP data is available for eight dates, and only one of those dates exactly matches a field date (23 June). To use L2_SM_SP data as a coarse resolution soil moisture input for the other field dates, data were temporally interpolated from the nearest available dates before and after. Temporal interpolation may introduce some uncertainty in the estimates because nonlinear changes in soil moisture that occur in between dates would not be captured. The interpolated product with a 3 km grid size was clipped to the 9 km modeling extent (Figure 1) and the spatial data was implemented into the EMT+VS model as the coarse resolution soil moisture input with multiple values.

Land Surface Models

A coarse soil moisture input to the EMT+VS model can also be obtained from land surface models. Data from the Noah and Mosaic were obtained from Phase 2 of North American

Land Data Assimilation System (NLDAS project, 2021). VIC data was also available for the study period but was ultimately not used because VIC drastically overestimated the average soil moisture conditions observed in the field. These products have hourly temporal resolutions and 1/8-degree spatial resolution (~12 km), coarser than the SMAP products used in this study. Like the SMAP L4 3-hourly model, the average of the hourly estimates from UTC 15-18 was used to correspond with early morning field data collection. Despite covering a region larger than SMAP, a single value from the Noah and Mosaic grid cell most closely aligned with the Maxwell Ranch boundary was used for the coarse resolution soil moisture input over the modeling extent.

4.2 Topography

Topographic inputs used for the EMT+VS model were derived from DEMs with resolutions of 30, 10, and 3 m. DEMs for Larimer County with 30 and 10 m resolutions were obtained via the Natural Resources Conservation Service (NRCS), which provides UTM-projected DEMs by county (USDA/NRCS). These DEMs are a part of the National Elevation Database (NED), which uses a mosaic of best-available elevation data from various sources. Additionally, a 1 m DEM from USGS is available for the study region, produced from high-resolution LiDAR source data (USGS, 2022). However, the finest resolution vegetation data available, discussed in the next section, is at a resolution of 3 m. Therefore, the 1 m DEM was resampled to a 3 m resolution to match the grid cell size of the finest vegetation and to reduce data processing. Each of these inputs were processed in ArcGIS Pro to obtain pit-removed elevation, slope, aspect, and contributing area using a combination of GIS tools and the TauDEM toolbox (Tarboton, 2003). Subsequently, curvature was calculated based on elevation (Heimsath et al., 1997) and PSRI was calculated based on latitude, slope, aspect, and day of year (Lee,

1964; Swift, 1976; Dingman, 2015). The day of the summer solstice was used for trials discussed in this study to correspond with the summer field campaign.

Coarser resolution DEMs are subject to more uncertainty because small-scale variations in topography are not captured. Additionally, errors in the initial elevation estimates propagate as the DEM is processed to obtain other attributes. Thompson et al. (2001) compared DEM-derived products at different resolutions (10 and 30 m) from different sources (field survey and USGS DEM, respectively). They found the coarsening DEM resolution caused more moderate slope gradients, underestimating slopes at steep locations and overestimating slopes at flatter locations, with the largest errors occurring on the extremes. Additionally, as DEM resolution coarsened, larger contributing areas were attributed to upper landscapes, and inversely, lower contributing areas were attributed to lower landscapes. Lastly, Thompson et al. (2001) noted that differences in source data makes the most difference when considering drainage pathways; the field survey DEM was better able to capture local depressions and more accurate flow paths than the USGS DEM. Erskine et al. (2007) investigated the sensitivity of terrain attributes to DEM resolution and found that bias and RMSEs of topographic attributes including slope, aspect, and curvature generally increased with increasing DEM grid size, with curvature being the most sensitive to resolution changes. Like Thompson et al. (2001), Erskine et al. (2007) also found that curvature values were reduced at coarser resolutions.

4.3 Vegetation

Various sources of multispectral satellite imagery are available from which fractional vegetation cover can be calculated. This study applies data from two primary sources: 10-m Sentinel-2 (ESA, 2022), and 3-m Planet Cube Sat (Planet Labs, 2022). Cloud-free images were available on different dates depending on the source. Sentinel-2 images were available on 26

May and 15 June 2022, and a Planet CubeSat image was available on 13 June 2022. The earliest available date after the start of the field campaign that began in late spring was preferred to represent a variety of conditions before summer storms saturated the site. Various indices can be used to estimate fractional vegetation cover, *V,* based on available multispectral bands from these three sources. In this study, *V* was characterized using Normalized NDVI, Normalized NDVI^2, SAVI, and EVI, which are described here.

The Normalized Difference Vegetation Index (NDVI), a common measure of vegetation greenness and health (Rouse et al., 1974), is calculated:

$$NDVI = \frac{NIR - RED}{NIR + RED} \tag{18}$$

where *NIR* and *RED* are the reflectances in the red and near-infrared bands. NDVI values range from +1 (dense green-leafy vegetation) to -1 (water bodies). However, many authors point out flaws in using NDVI as a direct measure of fractional vegetation cover, stating that NDVI values are highly sensitive to atmospheric effects and subject to errors due to soil brightness (Liu and Huete, 1995; Carlson and Ripley, 1997)

To account for these effects and to obtain an estimate for V between 0 and 1, negative values of NDVI are removed and not considered, and positive values are adjusted using the following normalization equation (Montandon and Small, 2008):

$$Normalized\ NDVI = \frac{NDVI_{pixel} - NDVI_0}{NDVI_\infty - NDVI_0} \tag{19}$$

where $NDVI_{pixel}$ is the NDVI value for each pixel, $NDVI_0$ is the bare soil NDVI, and $NDVI_\infty$ is the fully vegetated NDVI. $NDVI_0$ and $NDVI_\infty$, which are unique to each satellite platform, were determined by identifying locations with bare and fully vegetated soil in satellite photos. For the study region, $NDVI_0$ ranged from 0.12 to 0.25 (Table A3), which is larger than previous studies

that estimated $NDVI_0$ = ~0.05 (Gutman and Ignatov, 1998; Gan and Burges, 2006; Matsui et al., 2005; Li et al., 2003; Ek et al., 2003; Zeng et al., 2000); however, some studies suggest that $NDVI_0$ is often under-estimated which leads to an overestimation of V (Montandon and Small, 2008). $NDVI_\infty$ values at Maxwell Ranch ranged from 0.73 to 0.77, similar to previous studies. Timilsina et al. (2021) also assessed vegetation at a Colorado Front Range site and found $NDVI_\infty$ = 0.70. Overall, normalizing NDVI based on reference bare and fully vegetated pixels helps standardize NDVI values and enhances sensitivity to vegetation changes by removing soil background influence.

To further reduce soil background and enhance sensitivity to greenness, several authors have suggested a quadratic model for estimating V, which uses Normalized $NDVI^2$ (Carlson and Ripley, 1997; Choudhury et al., 1994):

$$Normalized\ NDVI^2 = \left(\frac{NDVI_{pixel} - NDVI_0}{NDVI_\infty - NDVI_0}\right)^2 \quad (20)$$

This method to estimate V allows for further amplification of the variations in vegetation from bare to highly vegetated soils and has been shown to result in lower overestimations of fractional vegetation cover (Montandon and Small, 2008).

The soil-adjusted vegetation index (SAVI) also corrects for the influence of soil brightness in regions with low vegetation. Like NDVI, SAVI is calculated using the red and near infrared bands, with the addition of a soil brightness correction factor, *L*:

$$SAVI = \frac{NIR - RED}{NIR + RED + L}(1 + L) \quad (21)$$

Huete et al. (1988), who originally proposed SAVI, assessed the influence of different *L* values and found that the optimal *L* depends on vegetation densities, generally ranging from $L = 1$ at low vegetation densities to $L = 0.25$ at higher densities. However, they recommend $L = 0.5$ for intermediate vegetation densities and state that using this adjustment is appropriate for most land

cover types and should offer an improvement from NDVI alone. For this reason, and because Maxwell Ranch has intermediate vegetation cover, $L = 0.5$ was selected for this study.

Lastly, the Enhanced Vegetation Index (EVI), another correction to NDVI, was assessed in this study for use in the EMT+VS model. EVI considers three hyperspectral bands (red, near infrared, and blue) and includes additional coefficients that reduce background canopy or atmospheric effects. EVI is calculated:

$$EVI = G \frac{NIR - RED}{NIR + C1 * RED - C2 * BLUE + L} \quad (22)$$

Coefficients *C1* and *C2* account for atmospheric resistance from aerosols, *L* adjusts for canopy background effect, and G is a gain factor that rescales EVI. Values for *G*, *C1*, *C2*, and *L* were set to 2.5, 6, 7.5, and 1, respectively, in accordance with Huete et al. (2002). EVI is shown to be more sensitive to densely vegetated regions in comparison to NDVI, which, despite capturing a similar range of values, asymptotically approaches a maximum and loses sensitivity to changes in highly vegetated regions (Huete et al., 2002).

5 MODEL TESTING AND EVALUATION

5.1 Performance Metrics

The performance of each trial is evaluated via RMSE, spatial NSCE, and space-time NSCE. RMSE is a simple metric that describes how far off the EMT+VS modeled predictions are from the actual values, on average. Spatial NSCE is calculated by averaging the NSCE on each date. Values of NSCE range between $-\infty$ and 1; a value of NSCE = 1 indicates a perfect match between observed and predicted data (Nash and Sutcliffe, 1970). When used to evaluate downscaling within a single coarse grid cell, any spatial NSCE above zero indicates that the fine resolution soil moisture is a better prediction of the soil moisture observations than the spatial average in the coarse grid cell, thus indicating a gain in accuracy due to downscaling. Space-time NSCE is a single NSCE calculated for all locations and dates at once, which also depicts the model's ability to capture temporal variability. This method generally reports higher values and might produce values above zero even if downscaling provides no value because space-time NSCE still captures some temporal variability. Cowley et al. (2017) also observed space-time NSCEs that were consistently higher than spatial NSCEs.

By construction, the spatial average of the EMT+VS model output should reproduce the coarse resolution input and therefore results in a mean bias error of zero, so long as observed soil moisture does not exceed the porosity specified by the model, which constrains the modeled estimates. If observed soil moisture does exceed the model-specified porosity, then the average of modeled estimates will not exactly reproduce the coarse average input, and bias will be nonzero but still small.

5.2 Calibration Procedure

For each set of model inputs, 17 single-value parameters describing the climate at the site, vegetation, and soil properties were specified or calibrated. For the scenarios discussed, only one parameter was directly specified: the thickness of the hydrologically active layer (δ_0), which was defined as 5 cm, the depth that soil moisture samples were taken. For the other 16 calibrated parameters, feasible ranges were assumed based physical constraints and prior work (Coleman and Niemann, 2013; Werbylo and Niemann, 2014; Ranney et al., 2015; Cowley et al., 2017; Hoehn et al., 2017; Grieco et al., 2018; Pauly et al., 2020). Calibration was conducted by generating random initial parameters within feasible ranges, then optimizing those parameters to achieve the maximum space-time NSCE, across all points and dates.

5.3 Comparative Methods

The performance of the EMT+VS model was compared with two alternative methods: OPTRAM, an optical fine-scale predictive method, and GeoWATCH, a physically based data assimilation downscaling method. These models were assessed using the Maxwell Ranch soil moisture dataset for performance comparison to the EMT+VS model results.

OPTRAM

OPTRAM, proposed in Sadeghi et al. (2017), is an optical method which estimates surface soil moisture based on the linear relationship between soil moisture and shortwave infrared transformed reflectance (STR), which is calculated from the shortwave-infrared band. Like the EMT+VS model, OPTRAM can accept optical data from Sentinel-2. Applying the OPTRAM method to Maxwell Ranch provides context for EMT+VS model performance.

Parameterization for the OPRAM model is based on ‘wet’ and ‘dry’ edges of the STR-NDVI space, whose scatter trapezoidal in shape. Sadeghi et al., (2017), in their original

description of OPTRAM, described that the model achieved an RMSE of 0.042 and 0.039 cm^3/cm^3 using Sentinel-2 data for two study sites, with 40 cloud-free images available for testing and validation. Because OPTRAM uses optical data, the model is limited to estimating soil moisture only on dates where cloud-free satellite images are available, which could result in significant data gaps as is illustrated in this study. At Maxwell Ranch, only two cloud-free Sentinel-2 images were available (26 May and 15 June) that closely corresponded to field dates. The OPTRAM method was applied as described by Sadeghi et al. (2017) using parameterization based on these two images. The output soil moisture estimates were validated with the respective field data on 27 May and 15 June 2022.

GeoWATCH

GeoWATCH is a comparable method to EMT+VS but has only been tested on a sparsely instrumented national scale or a heavily instrumented catchment scale national scale (Gambill et al., 2020; Eylander et al., 2023). GeoWATCH has not been evaluated at a larger and more diverse study region with abundant in-situ measurements, such as Maxwell Ranch. To assess the performance of GeoWATCH at Maxwell Ranch and fill this gap in knowledge, GeoWATCH data for surface soil moisture (0 – 10 cm depth) was obtained for all field dates, specifically for the 3-hr block from UTC 15-18. The GeoWATCH estimates, which provide 30 m gridded estimates, were evaluated against HydraProbe data at the corresponding sampling locations on all dates to provide comparison to the performance of the EMT+VS model.

6 RESULTS AND DISCUSSION

6.1 Evaluation of Downscaling Inputs

Each input used in the EMT+VS model is subject to varying degrees of uncertainty which may impact the error in the final downscaled estimates. Errors could be due to the derivation, resolution, or inevitable stochastic variations of a given input product. This section compares errors produced in soil moistures predicted by the EMT+VS model when implemented with different input sources for the coarse resolution soil moisture, fractional vegetation cover, and topography. Observed differences between different data sources are also discussed. Comparison metrics used include mean bias error (MBE), ratio of standard deviations (RSD) calculated as the standard deviation of the y-axis variable over the standard deviation of the x-axis variable, NSCE, and RMSE.

Coarse resolution Soil Moisture

Figure 4 compares the coarse resolution soil moisture sources to the average of the rover data on each date. The rover provides ground-based intermediate-scale measurements that cover much of Maxwell Ranch, so the average measured soil moisture is expected to provide the most accurate estimate of spatial average soil moisture. The other coarse resolution soil moisture datasets include the average of the in-situ HydraProbe data, three different SMAP products, and two NLDAS land-surface models.

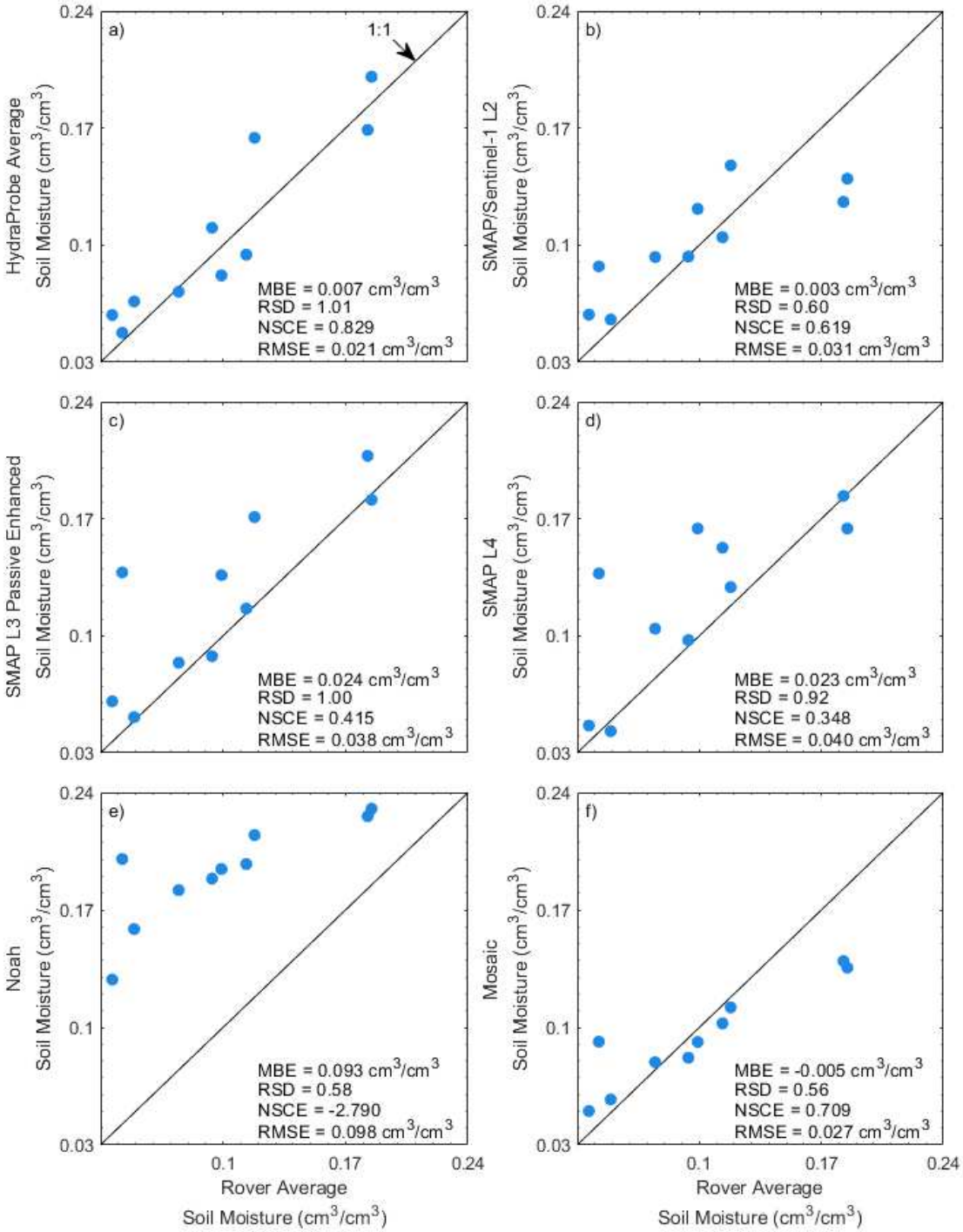

Figure 4. Comparison of coarse resolution soil moisture estimates to rover estimates with mean bias error (MBE), ratio of standard deviations (RSD), Nash-Sutcliffe coefficient of efficiency (NSCE), and root mean squared error (RMSE). Rover average soil moisture is on the x-axis for each plot. The y-axes show: (a) HydraProbe average soil moisture, (b) soil moisture from SMAP L2/Sentinel-1 product, (c) soil moisture from SMAP L3 Enhanced Passive product, (d) soil moisture from SMAP L4 product, (e) soil moisture from Noah land surface model, and (f) soil moisture from Mosaic land surface model.

Figure 4a illustrates that the spatial average soil moisture from the HydraProbes has the lowest error when compared to the rover average. The low error is partially expected because both datasets are from ground-based sensors collected over the same period each sampling day. However, the in-situ measurement locations were selected to capture diverse conditions within the study region, not to be representative of average conditions. The HydraProbes also measure soil moisture over 0-5 cm depth, whereas the rover is likely sensitive to deeper soil moisture; generally, the rover penetration depth varies from 12-76 cm depending on radial distance from the sensor and the soil moisture, although the rover measurements are most sensitive to near surface conditions (Köhli et al., 2015). Furthermore, the HydraProbe data collectively represent a miniscule portion of the study region. Nonetheless, the HydraProbe data have a small bias, a similar standard deviation to the rover data, and similar RMSE to the expected HydraProbe measurement error of ± 0.03 (Stevens Water, 2018).

Figure 4b compares the temporally interpolated Level 2 SMAP radiometer/Copernicus Sentinel-1 soil moisture values to the average values from the rover. Although the interpolated product has relatively small bias, the standard deviation is smaller than that of the rover data (RSD = 0.60). By interpolating in time, unobserved dates with extremely high and low soil moisture are poorly estimated. Nonetheless, the NSCE is high relative to the other products and the RMSE also remains relatively low. This SMAP product is expected to characterize the soil moisture in the top ~5 cm of the soil, while the rover is sensitive to deeper moisture. However, the difference in depths between these sensors is unlikely to cause substantial errors given the similarity of the HydraProbe and rover data shown earlier.

Figure 4c compares the soil moisture values from SMAP's Level 3 Passive Enhanced product to the average from the rover. This SMAP product tends to overestimate the spatial

average soil moisture (positive bias) but produces a similar range of soil moisture values (RSD = 1.00). SMAP's Level 3 Passive Enhanced product displays an RMSE that meets the SMAP mission requirement of <0.04 cm^3/cm^3 (Entekhabi et al., 2014).

Figure 4d compares the SMAP L4 soil moisture estimates to the average of the rover data. The Level 4 product displays a similar positive bias to the Level 3 product and underestimates the range of soil moisture values (RSD<1). The NSCE is low, which suggests that the temporal variations in the spatial average soil moisture are poorly captured. The RMSE of the Level 4 product is the highest among the SMAP products tested. As a model-derived product rather than a direct retrieval, SMAP L4 assimilates other relevant data sources, such as precipitation and meteorological information, and errors in those ancillary data or in the mathematical structure of the model could cause the higher RMSE in comparison to other SMAP products.

The average soil moisture from the Noah model greatly overestimates the spatial average soil moisture from the rover (Figure 4e). This result is consistent with other studies that have shown that Noah overestimates soil moisture in the top layer (Xia et al., 2015; Zhuo et al., 2015). The Noah model also underestimates the range of soil moisture values through time. The high RMSE and very negative NSCE of the Noah model indicate poor estimates of the rover data. Soil moisture estimates from the VIC model were also obtained from NLDAS-2 for the study region (not shown in Figure 4). VIC overestimates the spatial average soil moisture even more than Noah.

The Mosaic model (Figure 4f) provides much better estimates of the rover average soil moisture than the Noah model. The bias in estimates from the Mosaic model is small, but the model substantially underestimates the range of spatial average soil moisture values though time

(RSD = 0.56). Mosaic tends to overestimate the moisture during dry conditions and underestimate the moisture during wet conditions. Nonetheless, the soil moisture from the Mosaic model has the highest NSCE and lowest RMSE aside from the HydraProbe average. Overall, the results support Xia et al. (2015) who found that, out of the four NLDAS land surface models, Mosaic estimates had the lowest RMSE for surface soil moisture in Colorado, with a slight tendency for underestimation in wet soils.

Topography

Figure 5 compares the topographic attributes calculated at each sampling location from the three DEM resolutions (3 m, 10 m, and 30 m). For these plots, the attribute values from the 3 m DEM are displayed on the x-axis because they have the finest resolution. Of note, the source data differs between the 3 m DEM and the 10 and 30 m DEMs, which may also cause some differences between datasets.

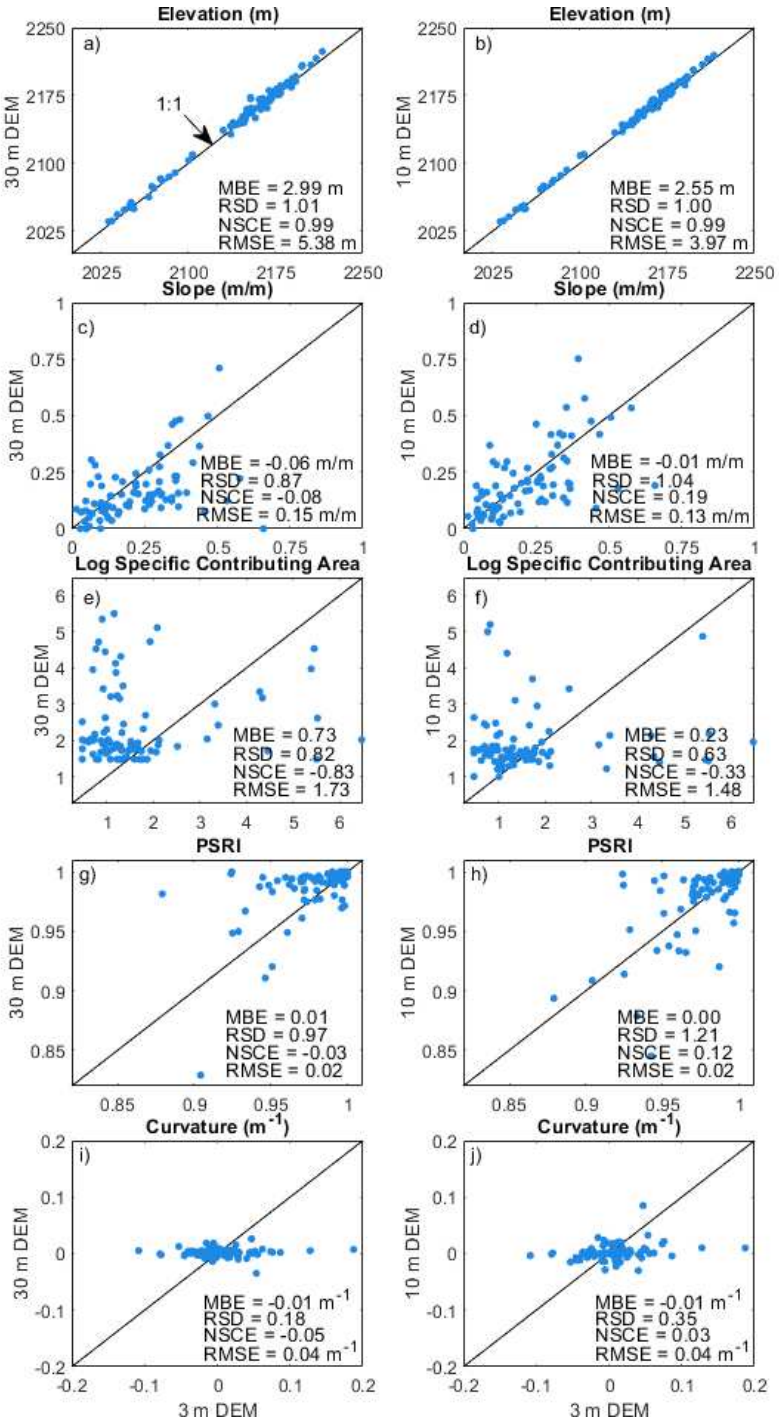

Figure 5. Comparison of topographic attributes from 30 m, 10 m, and 3 m DEMs with mean bias error (MBE), ratio of standard deviations (RSD), Nash-Sutcliffe coefficient of efficiency (NSCE), and root mean squared error (RMSE). Plots on the left compare attributes from the 30 m DEM to the 3 m DEM. Plots on the right compare attributes from the 10 m DEM to the 3 m DEM. Plots (a) and (b) compare elevations, plots (c) and (d) compare slope, plots (e) and (f) compare natural log of contributing area, plots (g) and (h) compare summer solstice potential solar radiation index (PSRI), and plots (i) and (j) compare curvature.

The elevation estimates at the sampling locations are very similar for all three DEM resolutions (Figure 5a and 5b). Both the 10 m and 30 m DEMs have small positive biases (~3 m), which might be due to different source data. In the EMT+VS model, elevation is used to model spatial variations in the potential ET. These results suggest that those variations would be similar for all three DEM resolutions.

The DEM resolution has a more notable effect on the slope values (Figure 5c and 5d). As the DEM resolution increases, the slopes are increasingly underestimated (more substantial negative biases), the range of slope values decreases (smaller RSD values), and RMSEs increase. These errors occur because local variations in slope are being averaged out due to the larger grid sizes. Erskine et al. (2007) had similar findings, noting reduced sensitivity to slope with increasing grid cell size and thus an increase in error, as well as a negative bias that increased with coarsening resolution. In the EMT+VS model, slope is used to calculate the hydraulic gradient for lateral flow and the PSRI for radiation ET. Because the slopes exhibit some scatter in these plots, those components of the model will also include errors. The most substantial errors may occur on steeper slopes that tend to be underestimated by the DEM.

Among all the attributes, specific contributing area exhibits the most substantial deviations around the 1:1 line for both the 30 m and 10 m data (Figure 5e and 5f), and the scatter is largest for large contributing areas. At finer resolutions, two adjacent cells can have vastly different contributing areas depending on small differences in the relative elevations of adjacent points and the implications on the d-infinity flow accumulation algorithm. On average, contributing areas are larger for the 30 m DEM but exhibit a smaller range of values, which also aligns with observations from the study by Thompson et al. (2001). In the EMT+VS model, contributing area is used to simulate the accumulation of flow due to lateral redistribution. The

scatter observed here suggests that the true pattern of lateral flow is difficult to estimate in practice.

Some scatter is observed in the PSRI values (which depend on the slope and aspect) when different DEM resolutions are used (Figure 5g and 5h). However, the performance metrics indicate small biases and small RMSE values. These results occur because most sampling locations have PSRI values near one (i.e., nearly flat locations) and those PSRI values are consistent among the different DEM resolutions. However, more disagreement occurs for points that have low PSRI values, due to changes in slope and aspect between DEMs. PSRI is used to calculate the spatial pattern of radiative ET. These results suggest that the largest errors in this pattern likely occur where PSRI is small, which typically occur on hillslopes.

Curvature is dramatically affected by changes in DEM resolution (Figure 5i and 5j). As resolution coarsens, the range of curvature values greatly decreases, and substantial scatter is observed. This behavior occurs because the curvature is being calculated over larger spatial scales. Erskine et al. (2007) found that curvature estimates are highly sensitive to DEM errors and suggests that finer resolution DEMs may not improve estimates of curvature; in fact, curvature estimates may be more accurate for coarser grid cell size. In the EMT+VS model, curvature is used to calculate the thickness of the hydrologically active layer, which affects lateral flow. In prior applications of the EMT+VS model, the model parameters have been consistently calibrated to minimize the dependence on curvature (and use a spatially constant layer thickness) (Cowley et. al, 2017; Grieco et al., 2018; Deshon et al., 2020). The errors in the calculated curvature values may explain dependance on curvature in prior EMT+VS applications has been minimal.

Vegetation

Figure 6 shows alternative estimates of fractional vegetation cover to compare the difference between vegetation indices, the date of the satellite image used, and the source satellite. Figures 6a and 6b compare SAVI and EVI with NDVI to assess differences between vegetation indices themselves if derived from the same image (Sentinel 2 image from 26 May 2022). Figure 6c compares values from two Sentinel-2 images on different dates (15 June vs. 26 May 2022) using normalized NDVI, whereas Figure 6d compares the same two dates but using the normalized $NDVI^2$ metric. Figures 6e and 6f compare satellite two satellite sources (Planet CubeSat and Sentinel-2) from similar dates (13 June and 15 June 2022) using both Normalized NDVI (Figure 6e) and Normalized $NDVI^2$ (Figure 6f). For these comparisons, Planet CubeSat (originally 3 m resolution) was upscaled to 10 m to match the resolution of the Sentinel-2 image.

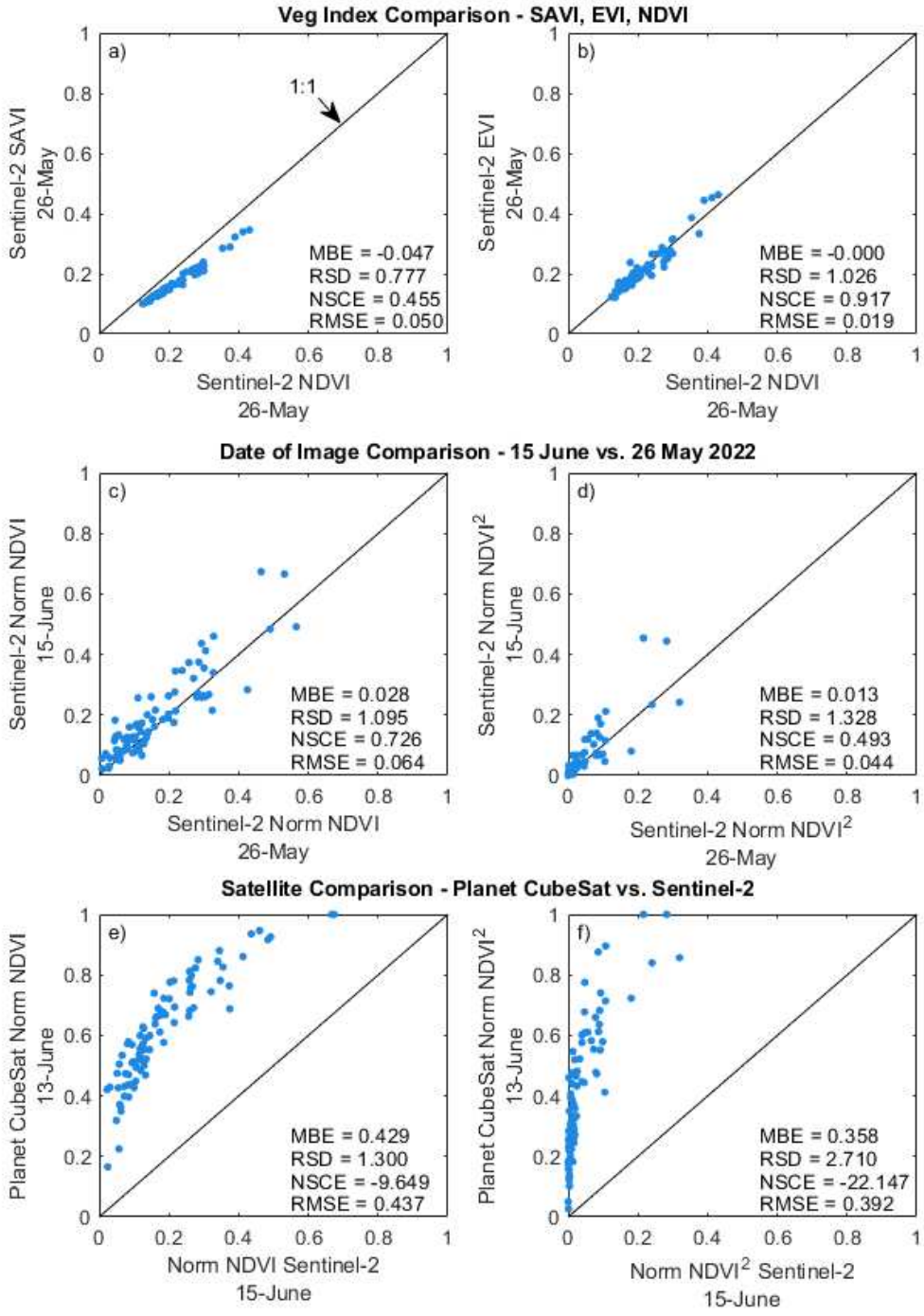

Fig. 6. Comparison of veg indices, satellite image date, and satellite source for estimating fractional vegetation cover (V) with mean bias error (MBE), ratio of standard deviations (RSD), Nash-Sutcliffe coefficient of efficiency (NSCE), and root mean squared error (RMSE). (a) Compares SAVI and NDVI from a Sentinel-2 image from 26 May 2022. (a) Compares EVI and NDVI from a Sentinel-2 image from 26 May 2022. (c) and (d) compare 15 June 2022 and 26 May 2022 Sentinel-2 images with both Normalized NDVI and Normalized $NDVI^2$. (e) and (f) compare a Planet CubeSat image from 13 June 2022 with a Sentinel-2 image from 26 May 2022 with Normalized NDVI and Normalized $NDVI^2$, respectively.

Figure 6a shows that SAVI estimates tend to be lower than NDVI, with an approximately linear transformation that has greater deviation for larger values. This difference in indices is due to the addition of the constant L in calculating SAVI (equation 21), which corrects NDVI for the influence of soil brightness and therefore tends to lower the values (Huete et al., 1988). Figure 6b shows that EVI and NDVI are more similar than SAVI and NDVI, with most points falling near the 1:1 line. However, EVI has a wider range (RSD > 1) and estimates larger values for highly vegetated regions because EVI is designed to be more sensitive to thicker vegetation (Huete et al., 2002).

Figure 6c shows a noticeable scatter between dates, with 15 June 2022 exhibiting a wider range of values than 26 May 2022. 15 June is a later (mid) summer date, and the ground has a higher water content because of precipitation events, increasing vegetation greenness, which also results in a positive bias. Squaring the Normalized NDVI metric in Figure 6d highlights a clearer distinction between highly vegetated locations and locations with moderate/low vegetation cover.

Figure 6e shows that Planet CubeSat estimates are substantially higher than Sentinel-2 using same vegetation index and nearby dates. The Planet CubeSat image from 13 June may have been greener than the Sentinel-2 image from 15 June because of drying that occurred between the two dates; however, Planet CubeSat lacks the radiometric quality of a larger satellite like Sentinel-2 and is made up of a constellation of small satellites that may suffer from inconsistencies (Houborg et al., 2018), so there is also the possibility that this deviation is more likely due to inconsistency between instruments. The nonlinear relationship shown in Figure 6e is mostly due to the resampling of Planet CubeSat data from 3 m to 10 m, a process which uses averaging and thus causes more values to fall in the middle range rather than the extremes.

Planet CubeSat has a much wider range of values, which is especially highlighted in Figure 6f, which shows Normalized $NDVI^2$ for both sources and reports a high RSD.

Failure to properly distinguish vegetation cover could lead to substantial errors in the EMT+VS model output. The influence of *V* in the EMT+VS model is highly controlled by the parameters that determine interception, shading, and transpiration effects. Depending on the calibrated parameters, higher vegetation could cause locations to be drier (through interception and transpiration) or wetter (due to shading).

6.2 Evaluation of Fine Resolution Soil Moisture for Base Case

A base case was developed using inputs that were anticipated to give the most accurate EMT+VS model estimates based on prior studies. For the coarse resolution soil moisture input, the spatial average soil moisture from the rover was selected. The 10 m DEM was used to describe the topography because the 3 m DEM required excessive computation times for repeated calibrations. Fractional vegetation cover was estimated from Sentinel-2 because the data product grid size matched the resolution of the DEM. A Sentinel-2 image from 26 May 2022 was selected for the base case because the fractional vegetation cover values distinguished the vegetation cover for both sparse and thickly vegetated areas without noticeable saturation. The fractional vegetation cover was calculated using normalized $NDVI^2$ (equation) to reduce overestimation of fractional vegetation cover (Montandon and Small, 2008).

To establish a base parameter set, the EMT+VS model was calibrated to the HydraProbe data from all dates and locations. The calibrated parameters are shown in Table A2. The soil moisture estimates from the EMT+VS model are determined as a weighted average of four underlying estimates, which are associated with aerodynamic ET, radiative ET, lateral flow, and deep drainage (equation 5). The weights associated with each estimate in the calibrated model

are plotted as a function of spatial average soil moisture in Figure 7. Aerodynamic ET has the highest influence on the soil moisture patterns for dry conditions. The soil moisture pattern from aerodynamic ET produces wetter conditions where vegetation is thicker because the vegetation shades the soil surface and reduces evaporation. For intermediate soil moisture values, radiative ET has the greatest weight. This soil moisture pattern depends not only on the vegetation pattern but also on the insolation, which depends on PSRI. Deep drainage becomes dominant only for the wettest conditions while lateral flow plays a secondary role for all conditions. Lateral flow produces wetter conditions in the valley bottoms where flow accumulates. The four maps in Figure 7 show the explicit solutions for aerodynamic ET, deep drainage, lateral flow, or radiative ET for 27 May 2022, which has an intermediate spatial average soil moisture value of 0.118 cm^3/cm^3. The maps show Region A because this sampling region exhibits the most topographic variation.

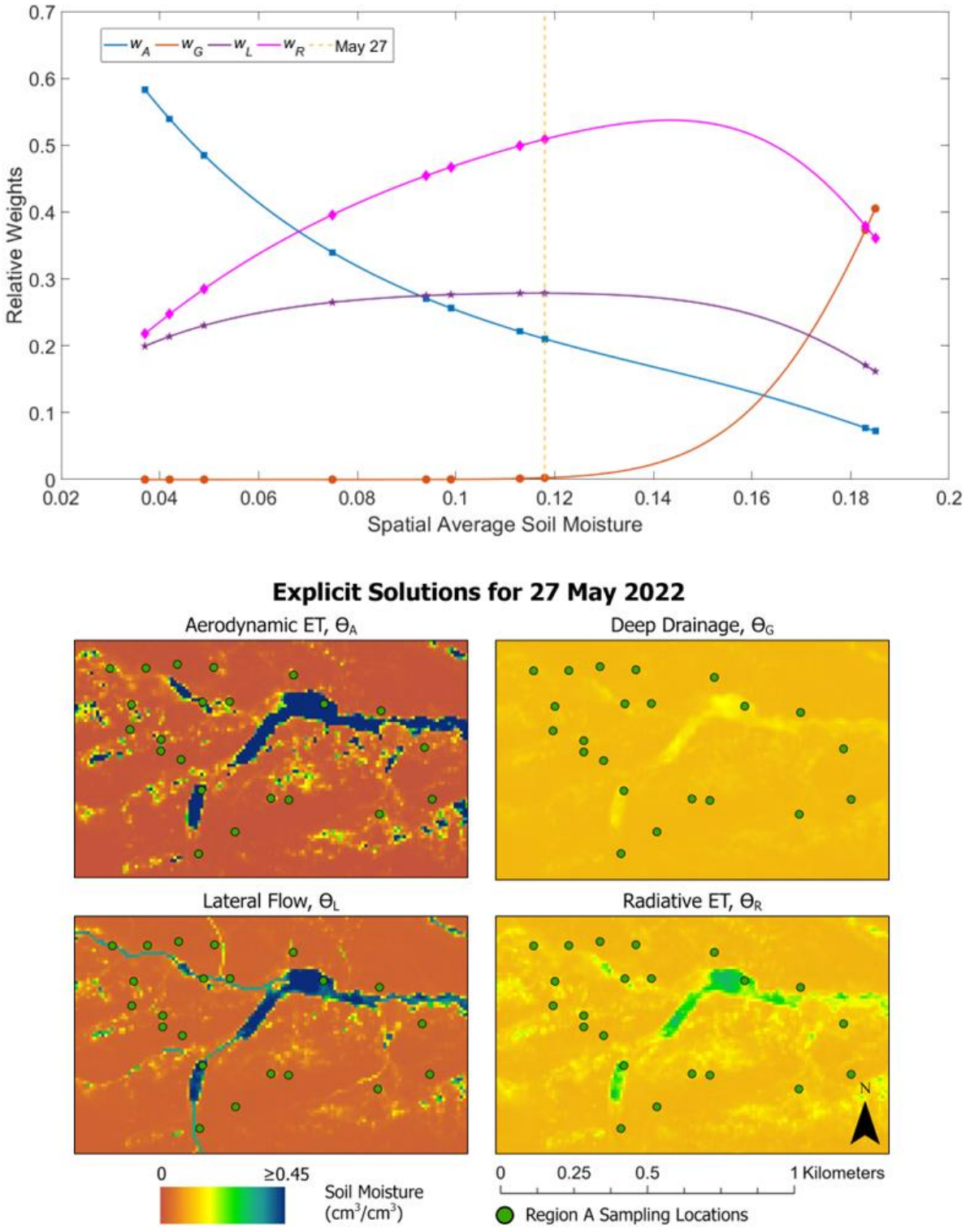

Figure 7. Relative weights plotted against spatial average soil moisture for base case EMT+VS model. Explicit solutions for aerodynamic ET, deep drainage, lateral flow, and radiative ET are shown for the highlighted date (27 May 2022) at Region A.

Maps of the EMT+VS soil moisture estimates for the base case are shown along with the HydraProbe measurements for all dates in Figure 8. Overall, the valley bottoms (which also tend to be more thickly vegetated) tend to be wet on all sampling dates. The rest of the study region has much drier conditions that generally follow the spatial average soil moisture through time. Despite the changing influence of aerodynamic ET, radiation ET, lateral flow, and deep drainage between dates, the spatial structure of the soil moisture pattern appears similar on all dates. This similarity occurs because thicker vegetation tends to occur in valley bottoms. Thus, the spatial patterns associated with the different processes are similar, since all four processes consider valley bottoms the wettest (as shown in the maps in Figure 7).

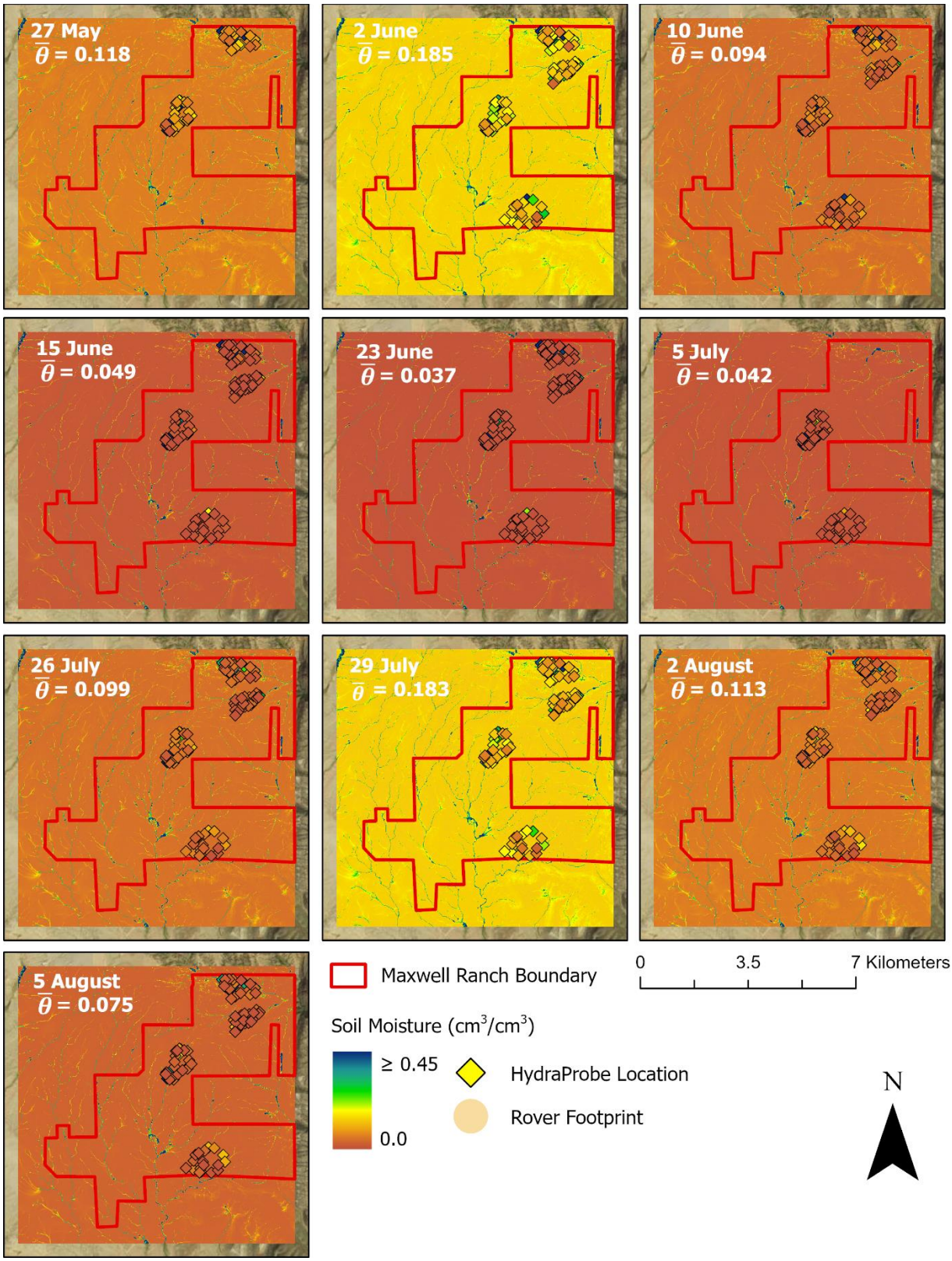

Figure 8. Fine resolution soil moisture maps from the base case EMT+VS model for all sampling dates, overlaid with ranch boundary and HydraProbe in-situ soil moisture measurements at sampling locations.

The soil moisture patterns from the base case have an overall RMSE of 0.077 cm^3/cm^3, an average spatial NSCE of 0.644, and an overall NSCE of 0.693. Previous studies have applied the EMT+VS model to smaller catchments and achieved RMSE values 0.028–0.047 cm^3/cm^3 (Ranney et al., 2015), as well as to larger regions and achieved RMSEs of 0.053–0.055 cm^3/cm^3 (Grieco et al., 2018). The high RMSE at Maxwell Ranch occurs in part due to the very wide range in in-situ soil moisture values. Soil moisture varies from 0 to 0.67 cm^3/cm^3, with the highest values occurring in peats that occur in some valley bottoms. The consistent secondary influence of lateral flow may also contribute to the higher errors because the lateral flow pattern is difficult to estimate accurately (as shown in the prior section). Despite the high RMSE, the NSCE values indicate that the model captures much of the spatial and space-time variability of the soil moisture. An additional validation experiment was performed in which 50% of the sampling locations were used for calibration and the remaining locations were used for evaluation, where each subset contained a diversity of soil, vegetation, and topographic characteristics. When applied in this manner, the RMSE for the evaluation dataset is 0.004 cm^3/cm^3 higher than the calibration RMSE, and the NSCE for the evaluation dataset is 0.08 lower than the calibration NSCE. This calibration/validation experiment shows that performance is similar whether using a subset of data or the entire dataset, provided that the subset is comparably heterogeneous to the full dataset. For simplicity, and to ensure the best performance possible, the entire dataset is used to both calibrate and validate the EMT+VS model throughout this study.

A direct comparison of each EMT+VS model estimate to corresponding HydraProbe measurement is shown in Figure 9 for the base case. Points represent measurements for all locations and dates, divided by subregion. Performance metrics are also reported by subregion.

Additionally, the map in Figure 9 shows squared error at each sampling location for 2 June 2022, overlaid on the map of log specific contributing area. 2 June 2022 had an overall RMSE of 0.094 cm^3/cm^3, the highest error of any individual date other than 27 May 2022 (RMSE = 0.099 cm^3/cm^3), which was an incomplete sampling day only capturing data for Regions A and B.

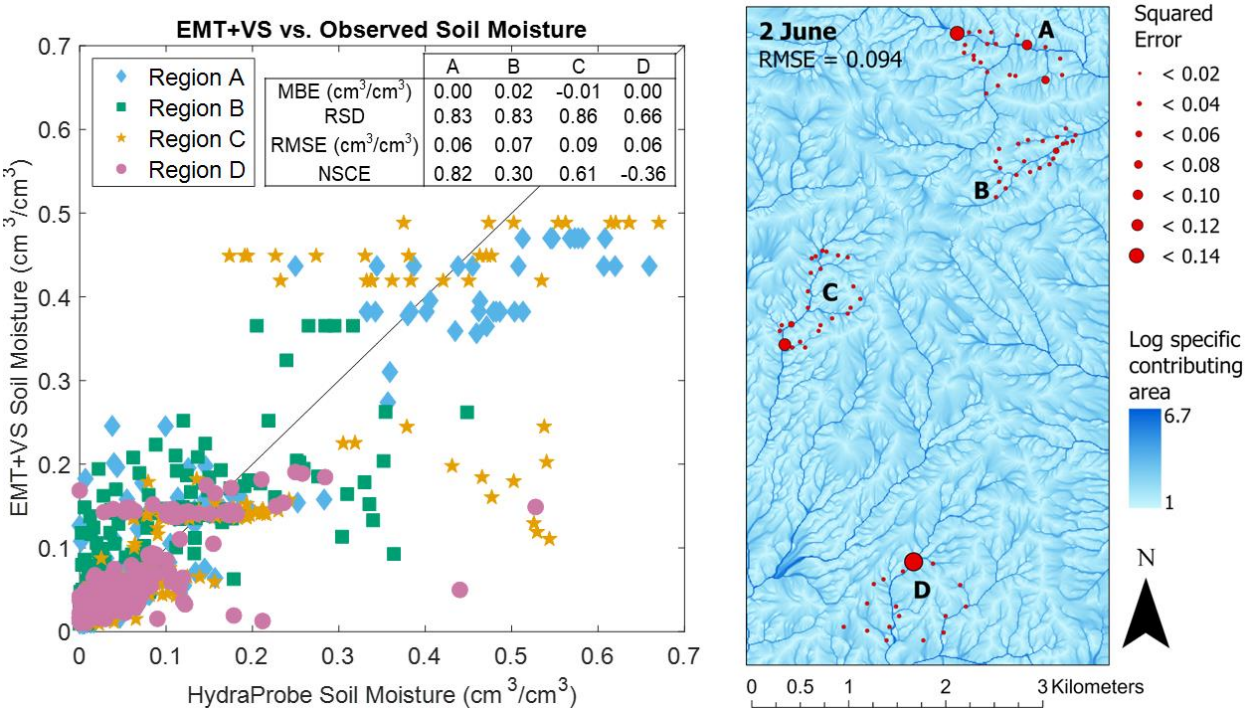

Figure 9. Base case EMT+VS soil moisture estimates plotted against HydraProbe soil moisture measurements for all sampling dates and locations (left) and map of squared error for 2 June 2022 for all sampling locations, overlaid on log specific contributing area map (right). 2 June 2022 had an RMSE of 0.094 cm^3/cm^3.

Figure 9 shows substantial scatter around the 1:1 line, which is consistent with the overall RMSE. The model has little bias for all four subregions because spatial average soil moisture from the rover is enforced. The EMT+VS model underestimates the spatial variability of soil moisture within each subregion (RSD < 1) because estimates near the average tend to produce lower errors than estimates that are extreme, so large variations may be reduced through calibration. A similar underestimation of the range of values was observed by Cowley et al. (2017). The RMSE values are similar among all four regions, while the NSCE values differ. The

best performance occurs in Region A because the region has highly variable topography and strong variations in vegetation cover, which produce strong and predictable spatial variations in soil moisture. Region B lacks very wet observations, which reduces the observed range of soil moisture values and thus the NSCE. Region C has several wet locations that are incorrectly predicted to be dry by the model, which occur at locations with thick vegetation that lie adjacent to a stream. These points are likely wet due to water loss from the stream (a dependence that is not represented by the model). Nonetheless, Region C has a wide range of soil moisture values that are mostly captured by the EMT+VS model and therefore a relatively large NSCE. NSCE is worst for Region D because this region has a small range of moisture conditions, but RMSE remains low. The map in Figure 9 indicates that the highest errors tend to occur at locations near drainage pathways or streams, likely due to errors in contributing area estimation or mischaracterization of vegetation cover in valley bottoms, which tend to be thickly vegetated. The map also shows that errors at most locations are low, but a few locations with high errors cause the overall RMSE to be large.

Another possible source of error in the soil moisture predictions is the assumption that the model parameters are constant over the entire study region. To explore how much heterogeneity affects the results, the EMT+VS model was calibrated separately for each region. The resulting RMSE values for Regions A, B, C, and D are 0.049, 0.055, 0.067, and 0.060 cm^3/cm^3 and the NSCE values are 0.917, 0.665, 0.822, and 0.402, respectively. The improved performance suggests that the parameters vary spatially over Maxwell Ranch. Spatial variations are most notable in the calibrated soil parameters, such as saturated hydraulic conductivity K_s, anisotropy ι, as well as horizontal and vertical pore disconnectedness indices γ_h and γ_v.

6.3 Comparison of Base Case Performance to Alternative Methods

If the coarse resolution soil moisture input for the base case (the rover average) is used as an estimator of the HydraProbe data (without downscaling), an RMSE of 0.132 (vs. 0.077 from the base case downscaled model) cm^3/cm^3 and an NSCE of 0.107 (vs. 0.693 from the base case downscaled model) are achieved. Therefore, downscaling using the EMT+VS model substantially improves accuracy of soil moisture. Additionally, two alternative soil moisture estimation methods, OPTRAM and GeoWATCH, were also applied to Maxwell Ranch and compared to the HydraProbe dataset.

The application of OPTRAM at Maxwell Ranch was limited to two dates because only two cloud-free Sentinel-2 images are available during the study period. Using the two available images (26 May and 15 June) and data from the closest sampling dates (27 May and 15 June), the OPTRAM method described by Sadeghi et al. (2017) produced RMSE values of 0.151 cm^3/cm^3 and 0.162 cm^3/cm^3 (vs. 0.099 and 0.076 from the base case downscaled model) and spatial NSCEs of 0.176 and -0.211 (vs. 0.650 and 0.730 from the base case downscaled model). A 1:1 plot of OPTRAM vs. HydraProbe soil moisture can be found in the appendix (Figure A1).

Several factors likely contribute to the weaker performance of OPTRAM. First, OPTRAM uses only multispectral data to estimate soil moisture, while the EMT+VS model uses a coarse resolution soil moisture value, multispectral data to estimate vegetation cover, and topographic data. Second, the EMT+VS model has a mechanistic basis, while OPTRAM is empirical. Third, even though OPTRAM does involve a type of calibration through identification of the wet and dry edges of the STR-NDVI space, OPTRAM is not calibrated to in-situ soil moisture observations like the EMT+VS model. This calibration is likely the most important reason that the EMT+VS model outperforms OPTRAM for these dates.

GeoWATCH estimates are available for all sampling dates. A 1:1 plot of GeoWATCH vs. HydraProbe soil moisture can be found in the appendix (Figure A2). Comparing to the HydraProbe data, GeoWATCH achieves an overall RMSE of 0.153 cm^3/cm^3 (vs. 0.077 from the base case downscaled model), an NSCE of -0.191 (vs. 0.693 from the base case downscaled model), and an average spatial NSCE of -0.453 (vs. 0.644 from the base case downscaled model). The higher NSCE than the average spatial NSCE suggests that GeoWATCH captures some of the temporal variability in the soil moisture observations but does not capture the observed spatial variations. GeoWATCH performs better on wetter dates than drier dates. For example, June 2nd was the wettest sampling date, and GeoWATCH performs the best on this date with a spatial NSCE of 0.125. GeoWATCH is expected to perform better for wet conditions because the model was developed primarily for use in mobility assessments, which are most concerned with wet conditions.

GeoWATCH's poor performance at Maxwell Ranch likely occurs for several reasons. First, GeoWATCH limits soil moisture to the range between assumed values for the wilting point and porosity. Across all dates, the minimum soil moisture prediction from GeoWATCH is 0.047 cm^3/cm^3, and the maximum predicted value is 0.465 cm^3/cm^3. However, the HydraProbe data ranges from 0 cm^3/cm^3 to 0.67 cm^3/cm^3. Second, GeoWATCH tends to overestimate soil moisture at Maxwell Ranch. The overestimation could be due to the deeper depths depth (0-10 cm) in GeoWATCH data inputs compared to the 0-5 cm captured by the HydraProbes. However, the rover is also sensitive to deeper moisture and produces similar results to the HydraProbes. Third, GeoWATCH uses data from a land surface model (Noah) that may have higher errors due to slightly coarser resolution and model structure. Fourth, GeoWATCH uses a 30 m DEM, whereas the EMT+VS model uses a 10 m DEM. Fifth, GeoWATCH's description of vegetation

relies primarily on landcover type rather than the multispectral imagery that is used to characterize vegetation density in the EMT+VS model. Sixth, GeoWATCH is not calibrated to the in-situ soil moisture observations.

Overall, the results suggest that the EMT+VS model predictions, despite their relatively high RMSE values, are more accurate than using OPTRAM and GeoWATCH at Maxwell Ranch. Additionally, using the coarse resolution soil moisture from the rover as an estimate of HydraProbe point data also outperforms OPTRAM and GeoWATCH, showing that these two methods do not improve performance despite their fine output resolutions.

6.4 Sensitivity to Inputs

This section discusses the performance of the EMT+VS model when the inputs are changed from the base case. For each change in the inputs, the EMT+VS model is run using (1) the base case parameters and (2) recalibrated parameters. The results from these trials are summarized in Figure 10.

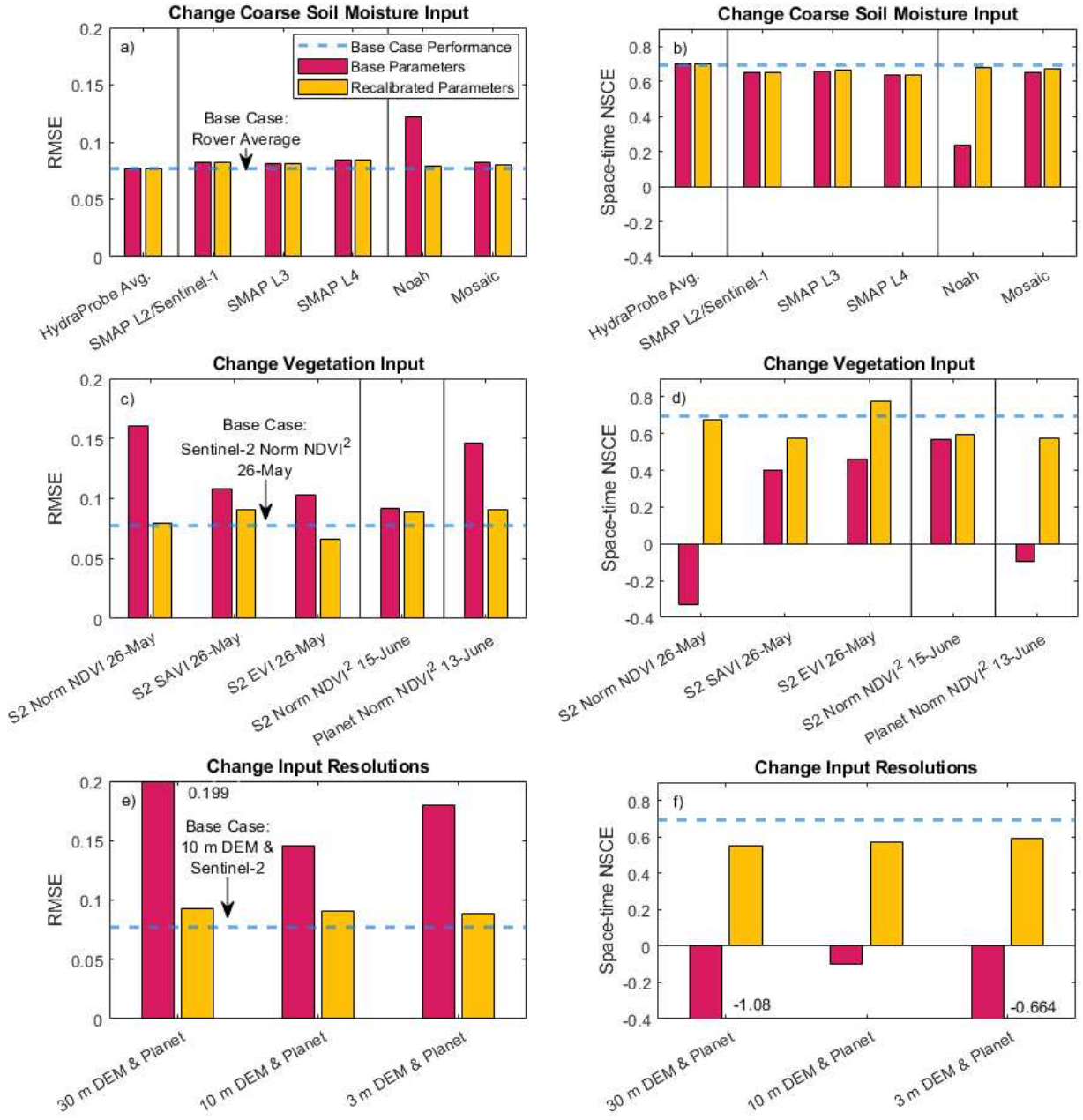

Figure 10. Performance comparison of EMT+VS model scenarios using base parameters and recalibrated parameters. Plots on the left show root mean squared error (RMSE), and plots on the right show Nash-Sutcliffe coefficient of efficiency (NSCE). Plots (a) and (b) depict results from trials where the coarse resolution soil moisture input was changed from the base case. Plots (c) and (d) depict results from trials where the vegetation input was changed. Plots (e) and (f) depict results from trials where the topography and vegetation resolution were changed.

Changing Coarse Resolution Soil Moisture

Figure 10a and 10b examine the effect of the coarse resolution soil moisture input on the EMT+VS model performance. Using the HydraProbe average instead of the rover average as the coarse resolution input results slightly better performance than the base case, and recalibration offers no improvement. The averages of the HydraProbe measurements are similar to the averages from the rover as shown in Figure 4, so similar performance is expected. When the SMAP products are used as inputs, the EMT+VS model achieves similar performance before and after recalibration but has slightly higher RMSEs and slightly lower NSCEs than the base case. Of the three SMAP products, SMAP L3 performs the best, followed by SMAP L2/Sentinel-1, and finally SMAP L4, but the differences are small. These differences in performance align with the errors observed in Figure 4 and show that higher errors in the inputs produce higher errors in the outputs. Recalibration only offers improvement for SMAP L3 to adjust for the positive bias.

Using the Noah land-surface model as the coarse resolution input results in much poorer EMT+VS model performance when the base parameters are used. The poor performance is expected given the large bias in the Noah soil moisture values observed in Figure 4. However, the EMT+VS model performance is substantially improved by recalibration, achieving an RMSE of 0.079 cm^3/cm^3, which is only slightly worse performance than the base case. When Mosaic is used as the coarse resolution input, the EMT+VS model performs similarly to when the SMAP products are used. Again, a slight improvement in performance occurs when the parameters are recalibrated, but the model still performs slightly worse than the base case. Overall, these results indicate that the EMT+VS model can achieve similar performance using a variety of coarse resolution soil moisture inputs. However, if the input has a substantial bias (like Noah), the parameters must be adjusted to compensate for that bias.

Changing Vegetation

Figure 10c and 10d examine the accuracy of the EMT+VS model soil moisture estimates when the vegetation pattern is estimated in different ways. Using (normalized) NDVI instead of (normalized) $NDVI^2$ (i.e., the base case) produces a substantial reduction in performance unless the parameters are recalibrated. After recalibration, the performance using NDVI (RMSE = 0.079 cm^3/cm^3) is similar to the performance using $NDVI^2$ (RMSE = 0.077 cm^3/cm^3). The index that is used to estimate the fractional vegetation cover (NDVI, SAVI, or EVI) has a substantial effect on EMT+VS model performance. SAVI produces worse performance than NDVI after both approaches are recalibrated. In contrast, EVI produces better performance than the base case after calibration (RMSE = 0.066 cm^3/cm^3). EVI might produce better performance than NDVI because NDVI becomes saturated in high biomass regions, whereas EVI is more sensitive to changes in vegetation density for these regions (Huete et al., 2002). A plot of the EMT+VS model estimates from the EVI case vs. the HydraProbe data is included in the Appendix, Figure A3. In comparison to Figure 9 (the base case), Figure A3 shows that the EVI case noticeably corrects for some underestimated points at Regions A, B and C, resulting in better overall performance. However, the positive bias of estimates at Region B is increased with the EVI case, possibly due to Region B's prominent forest cover where the shading effect causes points to be drier in reality than what is predicted by the model.

The date of the multispectral imagery that is used to estimate the vegetation cover also causes a noticeable change in EMT+VS model accuracy. Base case parameters were calibrated based on vegetation data from 26 May 2022, but when these parameters are applied in the model using satellite imagery from 15 June 2022, the accuracy of the soil moisture estimates reduces. With recalibration, performance improves but remains worse than the base case. This result suggests that the choice of date is important, and selecting a late spring date may be

advantageous to capture conditions before summer precipitation causes overall greener conditions.

The source of the multispectral data also affects the accuracy of the EMT+VS model soil moisture estimates. When Planet CubeSat data are coarsened to 10 m and used to calculate $NDVI^2$, they produce a much wider range of values as shown in Figure 5. The wider range produces much poorer accuracy in the soil moisture estimates unless the model parameters are recalibrated. Once the parameters are recalibrated, the soil moisture estimates have similar accuracy to those produced by Sentinel-2 using a nearby date (15 June 2022). Overall, the results suggest that the choice of vegetation index (NDVI, SAVI, EVI) affects the model results and that recalibration cannot completely overcome a poor choice. EVI produces the best performance. The date used to calculate the index also affects the accuracy of the EMT+VS model results.

Changing Input Resolution

In the prior analyses, the EMT+VS model was applied using 10 m data. Here, the model is also applied using 3 m and 30 m data (Figure 10e and 10f). To isolate the effect of the spatial resolution on the soil moisture estimates, a consistent multispectral dataset is used to estimate the fractional vegetation cover in all three cases. Specifically, Planet CubeSat data are used at 3 m, 10 m, and 30 m resolutions to estimate $NDVI^2$. Because the source of vegetation data has changed, the base case parameters produce poor soil moisture estimates at all three resolutions. With recalibration, however, performance improved for each case, and a small improvement in performance occurs as the resolution becomes finer. The 30 m, 10 m, and 3 m scenarios achieve RMSE values of 0.093 cm^3/cm^3, 0.091 cm^3/cm^3, and 0.089 cm^3/cm^3. The NSCEs for the 30 m, 10 m, and 3 m scenarios are 0.548, 0.575, and 0.595. These results suggest that the EMT+VS

model framework is applicable to finer resolutions than those considered previously. However, the computational cost of the running the 3 m model for only a slight improvement in performance could be reason to opt instead for the 10 m model.

7 CONCLUSIONS

In this study, the EMT+VS model was used to estimate fine resolution soil moisture patterns across a 6,000-ha study region with diverse topography, landcover types, and soils. The estimated soil moisture values were compared to in-situ measurements from HydraProbes at 86 locations on 10 dates. The sampling locations were selected to include diverse combinations of topographic and vegetation conditions and the sampling dates were selected to span the widest possible range of soil moisture conditions. For the conditions considered in this study, the following conclusions can be drawn:

1. The EMT+VS model successfully reproduces a substantial portion of the spatial and temporal variations in the in-situ soil moisture observations. The average spatial NSCE is 0.644, and the overall (space-time) NSCE value is 0.693. Nonetheless, the soil moisture estimates have higher errors for this study region (RMSE = 0.077 cm^3/cm^3) than the errors reported in prior applications of the EMT+VS model (RMSE values between 0.028 cm^3/cm^3 and 0.055 cm^3/cm^3). The errors are likely higher for this region in part because the soil moisture observations span a very wide range (0 to 0.67 cm^3/cm^3) due to soils varying from coarse sandy loams to peats. The errors may also be larger because the EMT+VS model parameters were assumed to be spatially constant across the region. Allowing spatial variations in the parameter values between subregions reduces the RMSE values to 0.049 to 0.067 cm^3/cm^3.
2. The EMT+VS model consistently produces more accurate estimates of the in-situ soil moisture observations at Maxwell Ranch than a coarse resolution input alone. The calibrated EMT+VS model also outperforms OPTRAM and GeoWATCH. The EMT+VS

model uses more sources of information than OPTRAM and can be directly calibrated to the in-situ soil moisture observations whereas OPTRAM is calibrated by estimating the wet and dry edges of the STR-NDVI space. OPTRAM also can only be applied for clear sky conditions. GeoWATCH typically overestimates the soil moisture in the study region; however, porosity constraint inhibits the ability of GeoWATCH to estimate soil moisture in wetlands or locations with organic soil, which are present at some sampling locations at Maxwell Ranch.

3. SMAP products provide reliable estimates of the spatial average soil moisture in the study region despite the variable topography. The RMSE values range from 0.031 cm^3/cm^3 to 0.040 cm^3/cm^3, which are in line with the SMAP mission requirements and other studies of SMAP performance (Entekhabi et al., 2014; Zeng et al., 2016; Chen et al., 2017; Chan et al., 2018). The SMAP L3 Passive Enhanced is more accurate than the SMAP/Sentinel-1 L2 product (which had to be interpolated in time to compare to the sampling dates) and the SMAP L4 product for the study region.
4. Among the tested land surface models from NLDAS-2 (Noah, Vic, and Mosaic), Mosaic produces the most accurate estimates of the spatial average soil moisture in the study region. Mosaic slightly overestimates dry conditions and underestimates wet conditions but has a lower RMSE than the SMAP L3 product. Noah and VIC both greatly overestimate the spatial average soil moisture in the region.
5. The EMT+VS model can achieve similar accuracies using diverse coarse resolution soil moisture inputs including the average of HydraProbe data, the average of cosmic ray neutron rover data, SMAP products, and land surface models from NDLAS-2. If the coarse resolution input contains substantial biases, the EMT+VS model parameters must

be adjusted to compensate. Otherwise, similar parameters can be used irrespective of the coarse resolution input.

6. The estimation of the fractional vegetation cover has a substantial impact on the accuracy of the EMT+VS model's soil moisture estimates. For the study region, using EVI to estimate the fractional vegetation cover produces more accurate estimates than using SAVI, NDVI, or $NDVI^2$. Estimating the fractional vegetation cover from imagery earlier in the spring produces more accurate soil moisture estimates than using a later spring image. Similar soil moisture accuracy is achieved using Sentinel-2 or Planet CubeSat imagery if both have 10 m resolution.
7. For the study region, the accuracy of the EMT+VS model results improve as the spatial resolution of the input data becomes more refined. The 10 m model outperforms the 30 m model, and the 3 m model outperforms the 10 m model. This behavior indicates that the representations of the hydrologic processes in the EMT+VS model are applicable down to 3 m and suggests that the EMT+VS model may be capable of producing 3 m soil moisture patterns in other regions.
8. Among the topographic attributes used in the EMT+VS model, contributing area and curvature exhibit the largest variations when calculated using DEMs with differing resolutions (3 m, 10 m, and 30 m). Slope and PRSI exhibit some scatter when compared between the resolutions, while elevation remains very consistent. Curvature typically plays a small role in the EMT+VS model, but contributing area is used (along with other variables) to determine the spatial variations in soil moisture due to lateral flow. The challenge of determining accurate contributing areas suggests that the EMT+VS model

may be less accurate when lateral flow is an important process in determining the soil moisture.

The results of this study inform future research needs. Future research should explore using unsupervised classification methods to determine subregions where EMT+VS model parameters can be considered spatially constant. Accounting for spatial variations in the parameters is expected to be more important when the EMT+VS model is applied across larger regions. Future studies should also consider downscaling intermediate scale soil moisture data from the cosmic ray neutron rover (in this study only the average of all rover data on a given date was downscaled). Studies should examine performance of the EMT+VS model in other regions (e.g., wetter climates) or the performance of other downscaling or soil moisture estimation technologies using the dataset from this study. Finally, studies could also consider combining benefits of multiple methods to improve fine resolution soil moisture estimation.

REFERENCES

Ahmad, S., Kalra, A., & Stephen, H. (2010). Estimating soil moisture using remote sensing data: A machine learning approach. *Advances in Water* Resources, *33(1),* 69-80. https://doi.org/10.1016/j.advwatres.2009.10.008

Ajami, H., & Sharma, A. (2018). Disaggregating soil moisture to finer spatial resolutions: A comparison of alternatives. *Water Resources Research, 54(11),* 9456-9483. https://doi.org/10.1029/2018WR022575

Alemohammad, S. H., Kolassa, J., Prigent, C., Aires, F., & Gentine, P. (2018). Global downscaling of remotely sensed soil moisture using neural networks. *Hydrology and Earth System Sciences, 22(10),* 5341-5356. https://doi.org/10.5194/hess-22-5341-2018

Bartalis, Z., Wagner, W., Naeimi, V., Hasenauer, S., Scipal, K., Bonekamp, H., ... & Anderson, C. (2007). Initial soil moisture retrievals from the METOP-A Advanced Scatterometer (ASCAT). *Geophysical Research Letters*, *34*(20). https://doi.org/10.1029/2007GL031088

Busch, F. A., Niemann, J. D., & Coleman, M. (2012). Evaluation of an empirical orthogonal function–based method to downscale soil moisture patterns based on topographical attributes. *Hydrological Processes, 26(18)*, 2696-2709. https://doi.org/10.1002/hyp.8363

Campbell, G. S. (1974). A simple method for determining unsaturated conductivity from moisture retention data. *Soil science, 117(6)*, 311-314. http://dx.doi.org/10.1097/00010694-197406000-00001

Carlson, T. (2007). An overview of the "triangle method" for estimating surface evapotranspiration and soil moisture from satellite imagery. *Sensors, 7(8)*, 1612-1629. https://doi.org/10.3390/s7081612

Carlson, T. N., & Ripley, D. A. (1997). On the relation between NDVI, fractional vegetation cover, and leaf area index. *Remote sensing of Environment, 62(3)*, 241-252. https://doi.org/10.1016/S0034-4257(97)00104-1

Chan, S. K., Bindlish, R., O'Neill, P., Jackson, T., Njoku, E., Dunbar, S., ... & Kerr, Y. (2018). Development and assessment of the SMAP enhanced passive soil moisture product. *Remote sensing of environment*, *204*, 931-941. https://doi.org/10.1016/j.rse.2017.08.025

Chen, Q., Miao, F., Wang, H., Xu, Z. X., Tang, Z., Yang, L., & Qi, S. (2020). Downscaling of satellite remote sensing soil moisture products over the Tibetan Plateau based on the random forest algorithm: Preliminary results. Earth and Space Science, 7(6), e2020EA001265. https://doi.org/10.1029/2020EA001265

Chen, Q., Zeng, J., Cui, C., Li, Z., Chen, K. S., Bai, X., & Xu, J. (2017). Soil moisture retrieval from SMAP: a validation and error analysis study using ground-based observations over the little Washita watershed. *IEEE Transactions on Geoscience and Remote Sensing*, *56*(3), 1394-1408. https://doi.org/10.1109/TGRS.2017.2762462

Choudhury, B. J., Ahmed, N. U., Idso, S. B., Reginato, R. J., & Daughtry, C. S. (1994). Relations between evaporation coefficients and vegetation indices studied by model simulations. *Remote sensing of environment*, *50*(1), 1-17. https://doi.org/10.1016/0034-4257(94)90090-6

Coleman, M. L., & Niemann, J. D. (2013). Controls on topographic dependence and temporal instability in catchment-scale soil moisture patterns. *Water Resources Research*, *49*(3), 1625-1642. https://doi.org/10.1002/wrcr.20159

Colliander, A., Jackson, T. J., Bindlish, R., Chan, S., Das, N., Kim, S. B., et al. (2017). Validation of SMAP surface soil moisture products with core validation sites. *Remote sensing of environment*, *191*, 215-231. https://doi.org/10.1016/j.rse.2017.01.021

Cowley, G. S., Niemann, J. D., Green, T. R., Seyfried, M. S., Jones, A. S., & Grazaitis, P. J. (2017). Impacts of precipitation and potential evapotranspiration patterns on downscaling soil moisture in regions with large topographic relief. *Water Resources Research*, *53*(2), 1553-1574. https://doi.org/10.1002/2016WR019907

Das, N. N., Entekhabi, D., Dunbar, R. S., Chaubell, M. J., Colliander, A., Yueh, S., et al. (2019). The SMAP and Copernicus Sentinel 1A/B microwave active-passive high resolution surface soil moisture product. *Remote Sensing of Environment*, *233*, 111380. https://doi.org/10.1016/j.rse.2019.111380

Das, N., D. Entekhabi, R. S. Dunbar, S. Kim, S. Yueh, A. Colliander, et al. (2020). SMAP/Sentinel-1 L2 Radiometer/Radar 30-Second Scene 3 km EASE-Grid Soil Moisture (Version 3) [Dataset]. Boulder, Colorado USA. NASA National Snow and Ice Data Center Distributed Active Archive Center. https://doi.org/10.5067/ASB0EQO2LYJV Date Accessed 01-31-2023

Desilets, D., Zreda, M., & Ferré, T. P. (2010). Nature's neutron probe: Land surface hydrology at an elusive scale with cosmic rays. *Water Resources Research*, *46*(11). https://doi.org/10.1029/2009WR008726

Dingman, S. L. (2015). *Physical hydrology* (pp. 571–577). Waveland Press.

Entekhabi, D., Yueh, S., & De Lannoy, G. (2014). SMAP handbook.

Erskine, R. H., Green, T. R., Ramirez, J. A., & MacDonald, L. H. (2007). Digital elevation accuracy and grid cell size: effects on estimated terrain attributes. *Soil Science Society of America Journal*, *71*(4), 1371-1380. https://doi.org/10.2136/sssaj2005.0142

European Space Agency. (2022). Sentinel-2 MSI-Level 2A [Dataset]. Copernicus Open Access. Retrieved from [https://scihub.copernicus.eu/]. Accessed 07-11-2022.

Eylander, J., Bieszczad, J., Ueckermann, M., Peters, J., Brooks, C., Audette, W., & Ekegren, M. (2023). Geospatial Weather Affected Terrain Conditions and Hazards (GeoWATCH) description and evaluation. *Environmental Modelling & Software*, *160*, 105606. https://doi.org/10.1016/j.envsoft.2022.105606

Fersch, B., Francke, T., Heistermann, M., Schrön, M., Döpper, V., Jakobi, J., ... & Oswald, S. (2020). A dense network of cosmic-ray neutron sensors for soil moisture observation in a highly instrumented pre-Alpine headwater catchment in Germany. *Earth System Science Data, 12(3), 2289-2309.* https://doi.org/10.5194/essd-12-2289-2020

Gambill, D. R., Wall, W. A., & Howard, H. R. (2020). Validation of the GeoWATCH soil moisture model and proposed bias correction method. *Journal of Terramechanics*, *91*, 1-9. https://doi.org/10.1016/j.jterra.2020.04.001

Grieco, N. R., Niemann, J. D., Green, T. R., Jones, A. S., & Grazaitis, P. J. (2018). Hydrologic downscaling of soil moisture using global data sets without site-specific calibration. *Journal of Hydrologic Engineering*, *23*(11), 04018048. https://doi.org/10.1061/(ASCE)HE.1943-5584.0001702

Heimsath, A. M., Dietrich, W. E., Nishiizumi, K., & Finkel, R. C. (1997). The soil production function and landscape equilibrium. *Nature*, *388*(6640), 358-361. https://doi.org/10.1038/41056

Hirschi, M., Seneviratne, S. I., Alexandrov, V., Boberg, F., Boroneant, C., Christensen, O. B., ... & Stepanek, P. (2011). Observational evidence for soil-moisture impact on hot extremes in southeastern Europe. *Nature Geoscience*, *4*(1), 17-21. https://doi.org/10.1038/ngeo1032

Houborg, R., & McCabe, M. F. (2018). A cubesat enabled spatio-temporal enhancement method (cestem) utilizing planet, landsat and modis data. *Remote Sensing of Environment*, *209*, 211-226. https://doi.org/10.1016/j.rse.2018.02.067

Huete, A. R. (1988). A soil-adjusted vegetation index (SAVI). *Remote sensing of environment*, *25*(3), 295-309. https://doi.org/10.1016/0034-4257(88)90106-X

Huete, A., Didan, K., Miura, T., Rodriguez, E. P., Gao, X., & Ferreira, L. G. (2002). Overview of the radiometric and biophysical performance of the MODIS vegetation indices. *Remote sensing of environment*, *83*(1-2), 195-213. https://doi.org/10.1016/S0034-4257(02)00096-2

Im, J., Park, S., Rhee, J., Baik, J., & Choi, M. (2016). Downscaling of AMSR-E soil moisture with MODIS products using machine learning approaches. *Environmental Earth Sciences*, *75*, 1-19. https://doi.org/10.1007/s12665-016-5917-6

Imaoka, K., Kachi, M., Kasahara, M., Ito, N., Nakagawa, K., & Oki, T. (2010). Instrument performance and calibration of AMSR-E and AMSR2. *International archives of the photogrammetry, remote sensing and spatial information science*, *38*(8), 13-18.

Ines, A. V., Das, N. N., Hansen, J. W., & Njoku, E. G. (2013). Assimilation of remotely sensed soil moisture and vegetation with a crop simulation model for maize yield prediction. Remote Sensing of Environment, 138, 149-164. https://doi.org/10.1016/j.rse.2013.07.018

Jin, Y., Ge, Y., Liu, Y., Chen, Y., Zhang, H., & Heuvelink, G. B. (2020). A machine learning-based geostatistical downscaling method for coarse-resolution soil moisture products. IEEE Journal of Selected Topics in Applied Earth Observations and Remote Sensing, 14, 1025-1037. https://doi.org/10.1109/JSTARS.2020.3035386

Kerr, Y. H., Waldteufel, P., Wigneron, J. P., Delwart, S., Cabot, F., Boutin, J., et al. (2010). The SMOS mission: New tool for monitoring key elements oft the global water cycle. *Proceedings of the IEEE*, *98*(5), 666-687. https://doi.org/10.1109/JPROC.2010.2043032

Köhli, M., Schrön, M., Zreda, M., Schmidt, U., Dietrich, P., & Zacharias, S. (2015). Footprint characteristics revised for field-scale soil moisture monitoring with cosmic-ray neutrons. *Water Resources Research*, *51*(7), 5772-5790. https://doi.org/10.1002/2015WR017169

Komma, J., Blöschl, G., & Reszler, C. (2008). Soil moisture updating by Ensemble Kalman Filtering in real-time flood forecasting. *Journal of Hydrology*, *357*(3-4), 228-242. https://doi.org/10.1016/j.jhydrol.2008.05.020

Koster, R. D., Guo, Z., Yang, R., Dirmeyer, P. A., Mitchell, K., & Puma, M. J. (2009). On the nature of soil moisture in land surface models. *Journal of Climate*, *22*(16), 4322-4335. https://doi.org/10.1175/2009JCLI2832.1

Krapez, J. C., Olioso, A., & Coudert, B. (2009, September). Comparison of three methods based on the temperature-NDVI diagram for soil moisture characterization. In *Remote Sensing for Agriculture, Ecosystems, and Hydrology XI* (Vol. 7472, pp. 220-231). SPIE. https://doi.org/10.1117/12.830451

Krishnan, P., Black, T. A., Grant, N. J., Barr, A. G., Hogg, E. T. H., Jassal, R. S., & Morgenstern, K. (2006). Impact of changing soil moisture distribution on net ecosystem productivity of a boreal aspen forest during and following drought. *Agricultural and Forest Meteorology*, *139*(3-4), 208-223. https://doi.org/10.1016/j.agrformet.2006.07.002

Lee, R. (1964). Potential insolation as a topoclimatic characteristic of drainage basins. *Hydrological Sciences Journal*, *9*(1), 27-41. https://doi.org/10.1080/02626666409493652

Legates, D. R., Mahmood, R., Levia, D. F., DeLiberty, T. L., Quiring, S. M., Houser, C., & Nelson, F. E. (2011). Soil moisture: A central and unifying theme in physical geography. *Progress in Physical Geography*, *35*(1), 65-86. https://doi.org/10.1177/0309133310386514

Liu, H. Q., & Huete, A. (1995). A feedback based modification of the NDVI to minimize canopy background and atmospheric noise. IEEE transactions on geoscience and remote sensing, 33(2), 457-465. https://doi.org/10.1109/TGRS.1995.8746027

Liu, Y., Jing, W., Wang, Q., & Xia, X. (2020a). Generating high-resolution daily soil moisture by using spatial downscaling techniques: A comparison of six machine learning algorithms. Advances in Water Resources, 141, 103601. https://doi.org/10.1016/j.advwatres.2020.103601

Liu, Y., Xia, X., Yao, L., Jing, W., Zhou, C., Huang, W., et al. (2020b). Downscaling satellite retrieved soil moisture using regression tree-based machine learning algorithms over Southwest France. *Earth and Space Science*, *7*(10). https://doi.org/10.1029/2020EA001267

Mascaro, G., Vivoni, E. R., & Deidda, R. (2010). Downscaling soil moisture in the southern Great Plains through a calibrated multifractal model for land surface modeling applications. *Water Resources Research*, *46*(8). https://doi.org/10.1029/2009WR008855

Montandon, L. M., & Small, E. E. (2008). The impact of soil reflectance on the quantification of the green vegetation fraction from NDVI. Remote Sensing of Environment, 112(4), 1835-1845. https://doi.org/10.1016/j.rse.2007.09.007

Moran, M. S., Clarke, T. R., Inoue, Y., & Vidal, A. (1994). Estimating crop water deficit using the relation between surface-air temperature and spectral vegetation index. *Remote sensing of environment*, 49(3), 246-263. https://doi.org/10.1016/0034-4257(94)90020-5

Nash, J. E., & Sutcliffe, J. V. (1970). River flow forecasting through conceptual models part I—A discussion of principles. *Journal of hydrology*, *10*(3), 282-290. https://doi.org/10.1016/0022-1694(70)90255-6

NLDAS project (2021), NLDAS Noah Land Surface Model L4 Hourly 0.125 x 0.125 degree V2.0 [Dataset], Edited by David M. Mocko, NASA/GSFC/HSL, Greenbelt, Maryland, USA, Goddard Earth Sciences Data and Information Services Center (GES DISC), 10.5067/T4OW83T8EXDO. Accessed 09-05-2023.

NLDAS project (2021), NLDAS Mosaic Land Surface Model L4 Hourly 0.125 x 0.125 degree V2.0 [Dataset], Edited by David M. Mocko, NASA/GSFC/HSL, Greenbelt, Maryland, USA, Goddard Earth Sciences Data and Information Services Center (GES DISC), 10.5067/TS58ZCJZIWT5. Accessed 09-05-2023.

NLDAS project (2021), NLDAS VIC Land Surface Model L4 Hourly 0.125 x 0.125 degree V2.0 [Dataset], Edited by David M. Mocko, NASA/GSFC/HSL, Greenbelt, Maryland, USA,

Goddard Earth Sciences Data and Information Services Center (GES DISC), 10.5067/45T7K120BJ2S. Accessed 11-01-2023.

O'Neill, P. E., S. Chan, E. G. Njoku, T. Jackson, R. Bindlish, J. Chaubell, and A. Colliander. (2021). SMAP Enhanced L3 Radiometer Global and Polar Grid Daily 9 km EASE-Grid Soil Moisture, Version 5 [Dataset]. Boulder, Colorado USA. NASA National Snow and Ice Data Center Distributed Active Archive Center. https://doi.org/10.5067/4DQ54OUIJ9DL.

Pauly, M. J., Niemann, J. D., Scalia, J., Green, T. R., Erskine, R. H., Jones, A. S., & Grazaitis, P. J. (2020). Enhanced hydrologic simulation may not improve downscaled soil moisture patterns without improved soil characterization. *Soil Science Society of America Journal*, *84*(3), 672-689. https://doi.org/10.1002/saj2.20052

Peng, J., Loew, A., Merlin, O., & Verhoest, N. E. (2017). A review of spatial downscaling of satellite remotely sensed soil moisture. *Reviews of Geophysics*, *55*(2), 341-366. https://doi.org/10.1002/2016RG000543

Planet Labs. (2022). Planet CubeSat Data [Dataset]. Retrieved from [https://www.planet.com/].

Priestley, C. H. B., & Taylor, R. J. (1972). On the assessment of surface heat flux and evaporation using large-scale parameters. *Monthly weather review*, *100*(2), 81-92. https://doi.org/10.1175/1520-0493(1972)100%3C0081:OTAOSH%3E2.3.CO;2

Pundir, S. K., & Garg, R. D. (2022). A comprehensive approachfor off-road trafficability evaluation and development of modified equation for estimation of RCI to assessregional soil variation using geospatial technology. *Quaternary Science Advances*, *5*, 100042. https://doi.org/10.1016/j.qsa.2021.100042

Ranney, K. J., Niemann, J. D., Lehman, B. M., Green, T. R., & Jones, A. S. (2015). A method to downscale soil moisture to fine resolutions using topographic, vegetation, and soil data. *Advances in Water Resources*, *76*, 81-96. https://doi.org/10.1016/j.advwatres.2014.12.003

Reichle, R., G. De Lannoy, R. D. Koster, W. T. Crow, J. S. Kimball, and Q. Liu. (2021). SMAP L4 Global 3-hourly 9 km EASE-Grid Surface and Root Zone Soil Moisture Analysis Update, Version 6 [Dataset]. Boulder, Colorado USA. NASA National Snow and Ice Data Center Distributed Active Archive Center. https://doi.org/10.5067/6P2EV47VMYPC. Date Accessed 10-18-2023.

Rezanezhad, F., Price, J. S., Quinton, W. L., Lennartz, B., Milojevic, T., & Van Cappellen, P. (2016). Structure of peat soils and implications for water storage, flow and solute transport: A review update for geochemists. *Chemical Geology*, *429*, 75-84. https://doi.org/10.1016/j.chemgeo.2016.03.010

Rouse Jr, J. W., Haas, R. H., Deering, D. W., Schell, J. A., & Harlan, J. C. (1974). *Monitoring the vernal advancement and retrogradation (green wave effect) of natural vegetation* (No. E75-10354). Retrieved from https://ntrs.nasa.gov/api/citations/19750020419/downloads/19750020419.pdf

Sabaghy, S., Walker, J. P., Renzullo, L. J., Akbar, R., Chan, S., Chaubell, J., ... & Yueh, S. (2020). Comprehensive analysis of alternative downscaled soil moisture products. *Remote Sensing of Environment*, *239*, 111586. https://doi.org/10.1016/j.rse.2019.111586

Sadeghi, M., Babaeian, E., Tuller, M., & Jones, S. B. (2017). The optical trapezoid model: A novel approach to remote sensing of soil moisture applied to Sentinel-2 and Landsat-8

observations. *Remote sensing of environment*, *198*, 52-68. https://doi.org/10.1016/j.rse.2017.05.041

Schrön, M., Rosolem, R., Köhli, M., Piussi, L., Schröter, I., Iwema, J., ... & Zacharias, S. (2018). Cosmic-ray neutron rover surveys of field soil moisture and the influence of roads. *Water Resources Research*, *54*(9), 6441-6459. https://doi.org/10.1029/2017WR021719

Schröter, I., Paasche, H., Doktor, D., Xu, X., Dietrich, P., & Wollschläger, U. (2017). Estimating soil moisture patterns with remote sensing and terrain data at the small catchment scale. *Vadose Zone Journal*, *16*(10), 1-21. https://doi.org/10.2136/vzj2017.01.0012

Soil Survey Staff, Natural Resources Conservation Service, United States Department of Agriculture. [Dataset] Web Soil Survey. https://websoilsurvey.nrcs.usda.gov/app/. Date Accessed 03-19-2023.

Srivastava, P. K., Han, D., Ramirez, M. R., & Islam, T. (2013). Machine learning techniques for downscaling SMOS satellite soil moisture using MODIS land surface temperature for hydrological application. *Water resources management*, *27*, 3127-3144. https://doi.org/10.1007/s11269-013-0337-9

Swift Jr, L. W. (1976). Algorithm for solar radiation on mountain slopes. *Water Resources Research*, *12*(1), 108-112. https://doi.org/10.1029/WR012i001p00108

Tarboton, D. G. (2003, July). Terrain analysis using digital elevation models in hydrology. In *23rd ESRI international users conference, San Diego, California* (Vol. 14). Retrieved from https://hydrology.usu.edu/dtarb/ESRI_paper_6_03.pdf

Thompson, J. A., Bell, J. C., & Butler, C. A. (2001). Digital elevation model resolution: effects on terrain attribute calculation and quantitative soil-landscape modeling. *Geoderma*, *100*(1-2), 67-89. https://doi.org/10.1016/S0016-7061(00)00081-1

Timilsina, S., Niemann, J. D., Rathburn, S. L., Rengers, F. K., & Nelson, P. A. (2021). Modeling hydrologic processes associated with soil saturation and debris flow initiation during the September 2013 storm, Colorado Front Range. *Landslides*, *18*, 1741-1759. https://doi.org/10.1007/s10346-020-01582-5

Trabucco, A., & Zomer, R. (2019). Global Aridity Index and Potential Evapotranspiration (ET0) Climate Database v2. figshare. [Dataset]. https://doi.org/10.6084/m9.figshare.7504448.v3 Date Accessed 02-09-2023.

USDA/NRCS, 2023. National Geospatial Center of Excellence. (n.d.). National Elevation Data 10 meter or better [Dataset]. Accessed 02-01-2023.

USDA/NRCS, 2023. National Geospatial Center of Excellence. (n.d.). National Elevation Data 30 meter [Dataset]. Accessed 02-01-2023.

U.S. Geological Survey, 2022. USGS 1 Meter 13 x48y453 CO_NorthwestCO_2020_D20 [Dataset]. Accessed 02-14-2023.

Wagner, W., Hahn, S., Kidd, R., Melzer, T., Bartalis, Z., Hasenauer, S., ... & Aubrecht, C. (2013). The ASCAT soil moisture product: a review of its. Meteorologische Zeitschrift, 22(1), 1-29. https://doi.org/10.1127/0941-2948/2013/0399

Walter, M. T., Steenhuis, T. S., Mehta, V. K., Thongs, D., Zion, M., & Schneiderman, E. (2002). Refined conceptualization of TOPMODEL for shallow subsurface flows. *Hydrological Processes*, *16*(10), 2041-2046. https://doi.org/10.1002/hyp.5030

Wei, Z., Meng, Y., Zhang, W., Peng, J., & Meng, L. (2019). Downscaling SMAP soil moisture estimation with gradient boosting decision tree regression over the Tibetan Plateau. *Remote Sensing of Environment*, *225*, 30-44. https://doi.org/10.1016/j.rse.2019.02.022

Werbylo, K. L., & Niemann, J. D. (2014). Evaluation of sampling techniques to characterize topographically-dependent variability for soil moisture downscaling. *Journal of Hydrology*, *516*, 304-316. https://doi.org/10.1016/j.jhydrol.2014.01.030

Xia, Y., Mitchell, K., Ek, M., Sheffield, J., Cosgrove, B., Wood, E., ... & Mocko, D. (2012). Continental-scale water and energy flux analysis and validation for the North American Land Data Assimilation System project phase 2 (NLDAS-2): 1. Intercomparison and application of model products. *Journal of Geophysical Research: Atmospheres*, *117*(D3). https://doi.org/10.1029/2011JD016048

Xia, Y., Ek, M. B., Wu, Y., Ford, T., & Quiring, S. M. (2015). Comparison of NLDAS-2 simulated and NASMD observed daily soil moisture. Part I: Comparison and analysis. Journal of Hydrometeorology, 16(5), 1962-1980.

Xu, W., Zhang, Z., Long, Z., & Qin, Q. (2021). Downscaling SMAP soil moisture products with convolutional neural network. *IEEE Journal of Selected Topics in Applied Earth Observations and Remote Sensing*, *14*, 4051-4062. https://doi.org/10.1109/JSTARS.2021.3069774

Zeng, J., Chen, K. S., Bi, H., & Chen, Q. (2016). A preliminary evaluation of the SMAP radiometer soil moisture product over United States and Europe using ground-based measurements. *IEEE Transactions on Geoscience and Remote Sensing*, *54*(8), 4929-4940. https://doi.org/10.1109/TGRS.2016.2553085

Zeng, X., Dickinson, R. E., Walker, A., Shaikh, M., DeFries, R. S., & Qi, J. (2000). Derivation and evaluation of global 1-km fractional vegetation cover data for land modeling. *Journal of Applied Meteorology*, *39*(6), 826-839. https://doi.org/10.1175/1520-0450(2000)039%3C0826:DAEOGK%3E2.0.CO;2

Zhao, W., Sánchez, N., Lu, H., & Li, A. (2018). A spatial downscaling approach for the SMAP passive surface soil moisture product using random forest regression. *Journal of hydrology*, *563*, 1009-1024. https://doi.org/10.1016/j.jhydrol.2018.06.081

Zhuo, L., Han, D., Dai, Q., Islam, T., & Srivastava, P. K. (2015). Appraisal of NLDAS-2 multi-model simulated soil moistures for hydrological modelling. Water Resources Management, 29, 3503-3517. https://doi.org/10.1007/s11269-015-1011-1

Zreda, M., Desilets, D., Ferré, T. P. A., & Scott, R. L. (2008). Measuring soil moisture content non-invasively at intermediate spatial scale using cosmic-ray neutrons. *Geophysical research letters*, *35*(21). https://doi.org/10.1029/2008GL035655

APPENDIX

Table A1. Summary of prior performance of EMT+VS model

Application Region	Depth Considered	Region Area	RMSE	Citation
Nerrigundah, New South Wales, Australia	15 cm	6 ha	0.047	2015
Cache la Poudre, Colorado, U.S.A.	5 cm	8 ha	0.028	2015
Tarrawarra, Victoria, Australia	30 cm	11 ha	0.028	2015
Satellite Station, North Island, New Zealand	30 cm	60 ha	0.048	2018
Drake Farm, Colorado, U.S.A.	15 cm	109 ha	0.026	2020
Reynolds Creek, Idaho, U.S.A.	5 cm	23,900 ha	0.055	2017
Tibet, Nagqu, China	5 cm	196,000 ha	0.053	2018

Table A2. Calibrated base case parameters

	lower	Calibrated optimized	upper	
V	gridded	gridded	gridded	Sentinel-2 Norm NDVI^2, 5/26
ϕ	0.2	0.33	0.45	Posority
γ_h	1	1.29	36	Horizontal pore disconnectedness
γ_v	6	13.80	36	Vertical pore disconnectedness
β_r	0.1	1.73	5	Radiative ET exponent
β_a	0.1	0.12	5	Aerodynamic ET exponent
α	0.1	0.10	0.4	Priestley-Taylor coefficient
ϵ	1	1.14	3	Relation of hydraulic to topographic gradient
η	0	0.47	1	Portion of transpiration from soil layer
K_s	1	3476.27	7000	Veritcal saturated hydraulic conductivity
ι	1	600.00	700	Anisotropy of saturated hydraulic conductivity
δ_o		0.05		Soil depth where topographic curvature is zero
κ_o	-999999	-9568.82	-0.3609	Minimum toporaphic curvature with soil
λ	0	0.999	0.999	Interception efficiency
μ	1	6.24	10	Shading effect on soil evaporation
PET	3	3.00	8	Potential evapotranspiration
ω	-0.0015	-0.0004	0.0015	PET elevation dependence
Veg-adj	0	0.50	0.50	Vegetation adjustment factor for porosity
		Space-time NSCE	0.693	
		Spatial Average NSCE	0.644	
		RMSE	0.0774	

Table A3. $NDVI_0$ and $NDVI_\infty$ for satellite sources

Source	$NDVI_0$		$NDVI_\infty$	
	Approx. Value	Location	Approx. Value	Location
Sentinel-2, 05/26	0.12	105.2405944°W 40.9416319°N	0.67	105.2623778°W 40.9085162°N
Sentinel-2, 06/15	0.13	105.2406160°W 40.9417069°N	0.73	105.2618416°W 40.9087143°N
PCS 06/13	0.25	105.2406906°W 40.9415804°N	0.77	105.2621636°W 40.9084000°N

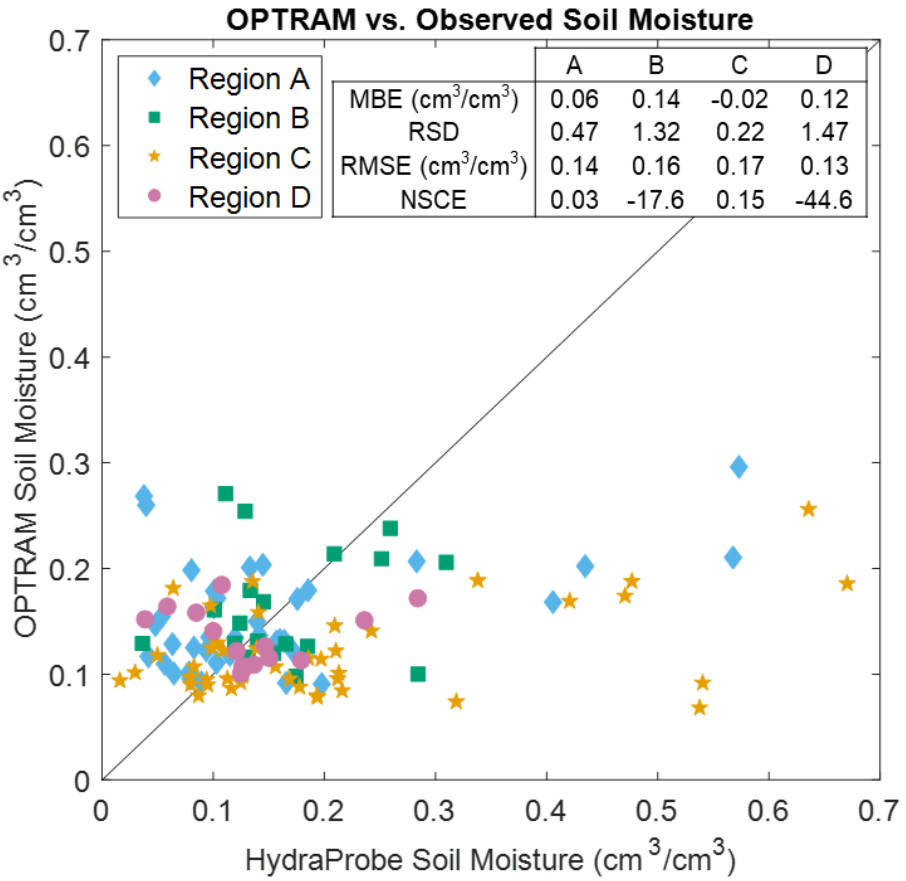

Figure A1. OPTRAM soil moisture estimates plotted against HydraProbe soil moisture measurements for 27 May and 15 June 2022 at sample locations.

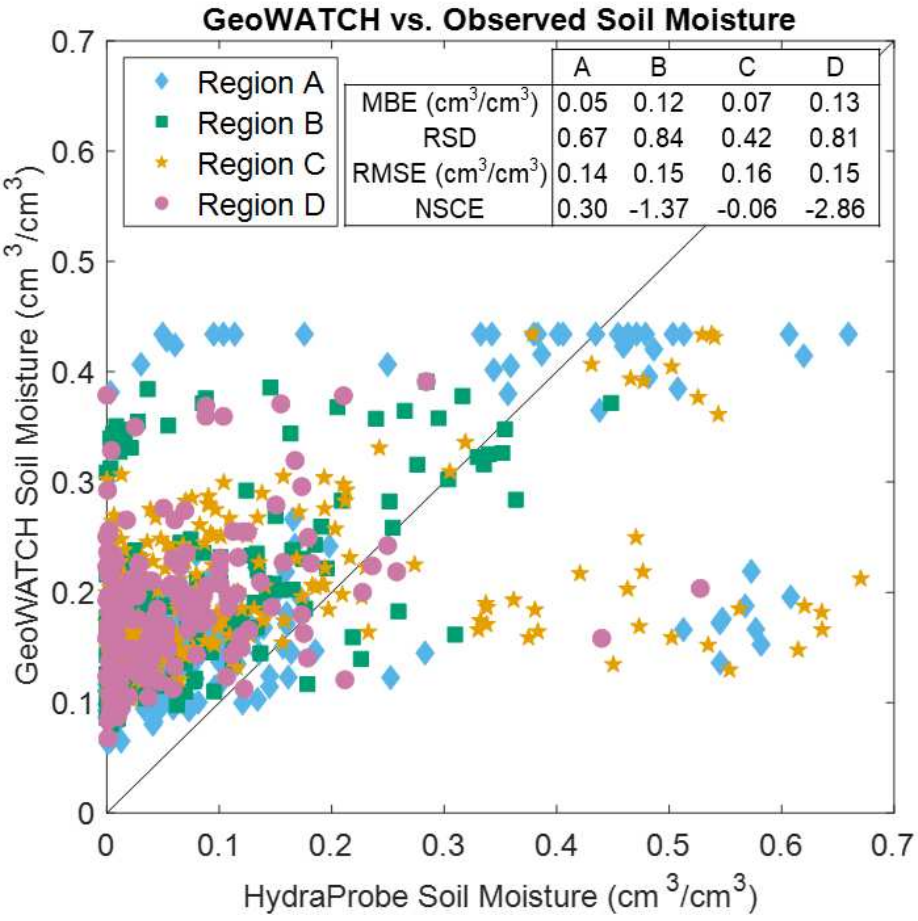

Figure A2. GeoWATCH soil moisture estimates plotted against HydraProbe soil moisture measurements for all sampling dates and locations.

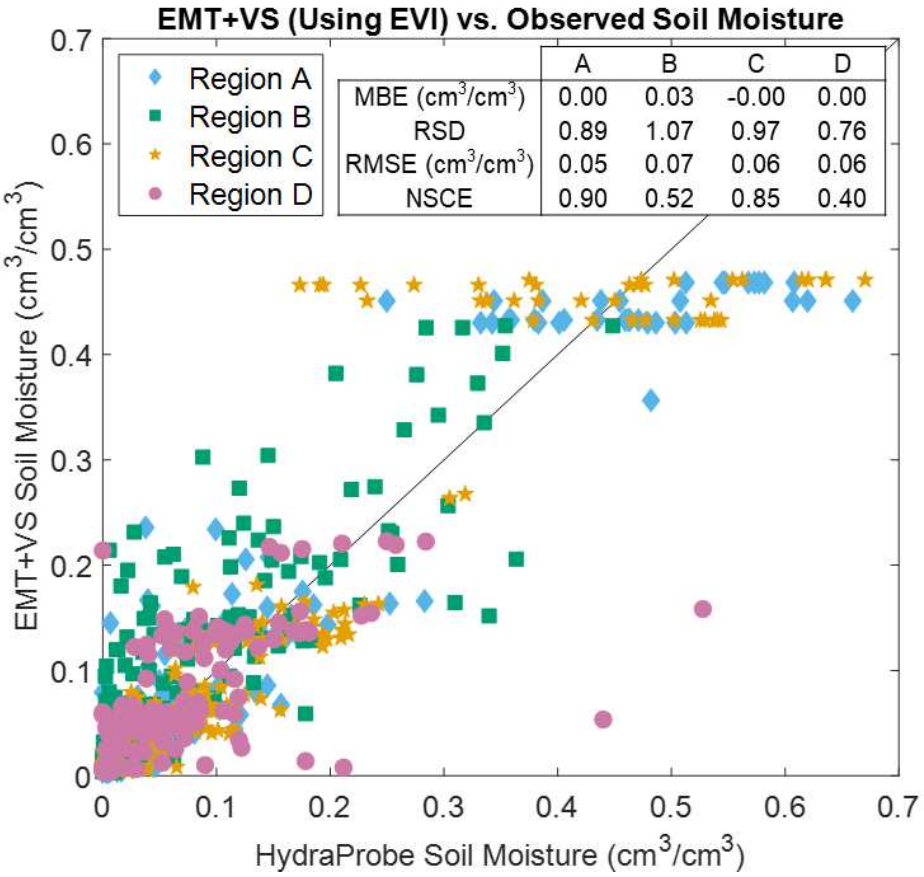

Figure A3. Soil moisture estimates from the EMT+VS model using EVI, plotted against HydraProbe soil moisture measurements for all sampling dates and locations.